Whole-cell FRET monitoring of transcription factor activities enables functional annotation of signal transduction systems in living bacteria

Received for publication, February 12, 2022, and in revised form, June 29, 2022 Published, Papers in Press, July 14, 2022,
https://doi.org/10.1016/j.jbc.2022.102258

Pengchao Wang[1,2], Guangming Zhang[1], Zeling Xu[1], Zhe Chen[1], Xiaohong Liu[3], Chenyin Wang[1], Chaogu Zheng[1], Jiangyun Wang[3,*], Hongmin Zhang[2,*], and Aixin Yan[1,*]

From the [1]School of Biological Sciences, The University of Hong Kong, Hong Kong, China; [2]Department of Biology, School of Life Sciences, Southern University of Science and Technology, Shenzhen, Guangdong, China; [3]Institute of Biophysics, Chinese Academy of Sciences, Beijing, China

Edited by Patrick Sung

Bacteria adapt to their constantly changing environments largely by transcriptional regulation through the activities of various transcription factors (TFs). However, techniques that monitor TF–promoter interactions *in situ* in living bacteria are lacking. Herein, we developed a whole-cell TF–promoter binding assay based on the intermolecular FRET between an unnatural amino acid, L-(7-hydroxycoumarin-4-yl) ethylglycine, which labels TFs with bright fluorescence through genetic encoding (donor fluorophore) and the live cell nucleic acid stain SYTO 9 (acceptor fluorophore). We show that this new FRET pair monitors the intricate TF–promoter interactions elicited by various types of signal transduction systems, including one-component (CueR) and two-component systems (BasSR and PhoPQ), in bacteria with high specificity and sensitivity. We demonstrate that robust CouA incorporation and FRET occurrence is achieved in all these regulatory systems based on either the crystal structures of TFs or their simulated structures, if 3D structures of the TFs were unavailable. Furthermore, using CueR and PhoPQ systems as models, we demonstrate that the whole-cell FRET assay is applicable for the identification and validation of complex regulatory circuit and novel modulators of regulatory systems of interest. Finally, we show that the FRET system is applicable for single-cell analysis and monitoring TF activities in *Escherichia coli* colonizing a *Caenorhabditis elegans* host. In conclusion, we established a tractable and sensitive TF–promoter binding assay, which not only complements currently available approaches for DNA–protein interactions but also provides novel opportunities for functional annotation of bacterial signal transduction systems and studies of the bacteria–host interface.

Pathogenic bacteria encounter diverse environmental and physiological stresses in their natural habitats and during infection of the human hosts, such as oxygen fluctuation, nutrient scarce, hyperosmolarity, bile salts, bactericidal agents, and so on (1). To survive these hostile environments, pathogens have developed exquisite regulatory systems that not only sense the diverse signals but also trigger specific responses by altering gene expression (1–3). In bacteria, stress adaption is largely achieved by regulation at transcriptional level through the activities of various transcription factors (TFs) (4). Efficient recognition and specific binding of TFs to their targeting promoters is the key for the success of stress adaptation and survival of the pathogens. However, a method to monitor the *in situ* TF–promoter binding in living bacteria, especially in the complex cellular environments under stresses, is lacking.

Owing to its importance in transcription regulation and stress adaptation, several methods to characterize the TF–promoter interactions, including both *in vitro* and *in vivo*, low and high throughput, have been developed. *In vitro* methods include the well-established EMSA (5, 6), filter-binding assay (7), DNA footprinting (8), isothermal titration calorimetry (9), and surface plasmon resonance (10), and others that detect the direct binding of TF to its promoters qualitatively and quantitatively. However, a common drawback of these *in vitro* methods is that the protein and DNA concentrations utilized are usually higher than those in the cell, and the DNA fragment is in naked form instead of the compact chromatin state in the cell. Hence, these methods are unable to precisely recapitulate the TF–promoter recognition and binding during the stress adaptation processes in living cells. The high-throughput approaches developed in recent years such as chromatin immunoprecipitation coupled with sequencing and systematic evolution of ligands by exponential enrichment are capable of capturing the TF–promoter binding *in vivo* occurred under specific culture conditions (11, 12). However, they are generally employed to provide a snapshot of the TF-binding sites in the entire genome of bacterial cells, and the techniques rely on high-throughput sequencing facilities, limiting their accessibilities and applications for targeted molecular studies. Furthermore, all these currently available methods are incapable of monitoring TF activities elicited by indirect or transient stimulants frequently generated during stress adaptation in living bacteria.

* For correspondence: Aixin Yan, ayan8@hku.hk; Hongmin Zhang, zhanghm@sustech.edu.cn; Jiangyun Wang, jwang@ibp.ac.cn.
Present address for Zeling Xu: Integrative Microbiology Research Centre, South China Agricultural University, Guangzhou, Guangdong, China.

Whole-cell FRET monitoring of TF–promoter interactions

FRET measurement is an extensively employed strategy to monitor conformational changes and associations between macromolecules in living organisms in real time (13–15). It measures the dipole–dipole energy transfer between two fluorophores (a donor and an acceptor) that are attached to the same biomolecule (intramolecular FRET) or a pair of biomolecules of interests (intermolecular FRET), respectively, when they are in nanoscale proximity and have spectral overlap. Since the efficiency of the energy transfer is reversely correlated to the six power of the distance of the two fluorophores (16), FRET measurement reliably indicates the close proximity and alignment of the macromolecule linker (intramolecular FRET) or macromolecule pairs (intermolecular FRET) onto which the donor and acceptor fluorophores are attached with extreme sensitivity and accuracy. Furthermore, FRET spectroscopy and microscopy represents almost the most simple and accessible form of super-resolved optical measurement (17–19), enabling quantitative and *in situ* characterization of macromolecule associations both *in vitro* and in living organisms. Attempts to measure protein–DNA interaction by FRET technique have been reported (20–23). However, majority of these assays were developed for measurement of protein–DNA fragment interactions *in vitro* because of the simplicity of fluorescent labeling of synthetic DNA fragments and recombinant proteins. Furthermore, intramolecular FRET in which the donor and acceptor fluorophores were dually attached to a single biomolecule was often employed, and protein–DNA interaction was inferred by the conformational changes of the fluorescently labeled single DNA or protein component (23, 24). These approaches are indirect and inapplicable to monitor the TF–promoter DNA binding in the complex cellular environments in living cells. Intermolecular FRET, on the other hand, is ideal to report the direct interaction of two macromolecules onto which the FRET fluorophore pairs are attached separately. Despite this advantage, an intermolecular FRET-based assay to detect macromolecule interactions in living cells is technically challenging because of the exquisite sensitivity of FRET, which requires both the close proximity and optimal alignment of the donor and acceptor pairs and controlling of the ratio of the donor and acceptor fusions to minimize background noise.

In this study, we design an intermolecular FRET-based assay system to monitor the intricate TF–promoter binding in living bacteria by separately labeling the TF protein and cellular chromosome DNA with a pair of bright fluorophores. To enable FRET measurement of living cells, we introduce fluorescence property into TF proteins through genetic encoding of a fluorescent unnatural amino acid (FUAA) at a defined site, that is, the DNA-binding domain (DBD) of TF proteins, as the donor fluorophore (25), and stain cellular chromosomal DNA employing a cell-permeable nucleic acid dye SYTO 9, which is highly selective to DNA molecules (extinction coefficient $>$50,000 cm^{-1} M^{-1}) with a substantial quantum yield (0.58) as the acceptor fluorophore (24). To establish a complementary fluorophore that pairs with SYTO 9, we compared the fluorescence properties of a handful of FUAAs with available aminoacyl-tRNA synthetase–tRNA pairs, which are required for genetic incorporation (Table S1) (26–31). An FUAA with the 7-hydroxycoumarin fluorophore, L-(7-hydroxycoumarin-4-yl) ethylglycine (CouA), which is characterized by an emission spectrum peaked at 450 nm with a high quantum yield (0.63) (26), displays the desired properties for spectral overlap with the DNA-bound SYTO 9 (absorption peak ∼500 nm). Moreover, the fluorophore affords a large Stokes shift (26) (Fig. S1), which is ideal for intermolecular FRET sensors because of free or minimal cross-excitation. The theoretical Förster radius of this new FRET pair (CouA–SYTO 9) is calculated to be 52.5 Å (Fig. S1), which should allow the occurrence of FRET when the distance between the two fluorophores is in the range of ∼25 to 75 Å.

Herein, we first validated the applicability and efficiency of the new FRET pair CouA–SYTO 9 to report the intricate TF–promoter interactions *in vitro* using a canonical TF–promoter system composed of the TF protein CueR (CueR–F58CouA) and its targeting promoter fragment P_{copA} stained by SYTO 9. An intermolecular FRET-based whole-cell assay was then established to measure the CueR–promoter interaction in living *Escherichia coli* cells in response to various direct and indirect stimulants. Specificity of the assay was verified by the abolishment of FRET upon mutating key arginine residues responsible for promoter binding in CueR or deleting all known targeting promoters of CueR (P_{copA} and P_{cueO}) in the chromosome of *E. coli*. Followingly, we extended the assay to monitor the signal transduction and transcription regulation elicited by two-component systems (TCSs) and to identify novel signals that modulate the regulatory systems of interest. Finally, we demonstrated that the FRET-based assay is applicable for single-cell analysis, and monitoring the TF activities in *E. coli* colonized in the *Caenorhabditis elegans* host.

Results

CouA is successfully incorporated into a canonical TF protein CueR at a defined site

To establish a TF–promoter binding assay based on intermolecular FRET, we first explored site-specific incorporation of CouA into the DBD of a canonical TF protein CueR, which displays intricate interactions with its targeting promoters during the switch from a transcription repressor to an activator upon signal sensing. CueR is a copper (Cu) and silver (Ag) metalloregulatory MerR family protein that senses Cu(I) stress and activates the expression of two target genes, *copA* and *cueO*, which encodes the ATPase copper exporter CopA and copper oxidase CueO, respectively (32–34) (Fig. 1*A*). The mechanism of transcription regulation by CueR has been elucidated by both crystallography in which CueR is bound with a 23-bp promoter DNA (35) and by cryo-EM in which CueR, RNAP, and a 58-bp promoter DNA forms a complex (36). These structural studies have suggested that CueR binds to target promoters and activates gene transcription by allosteric DNA distortion. Since CouA contains an aromatic side chain, we first selected aromatic amino acid residues located at the relatively unstructured loop regions in the DBD of CueR as the potential sites for CouA incorporation. The DBD of CueR

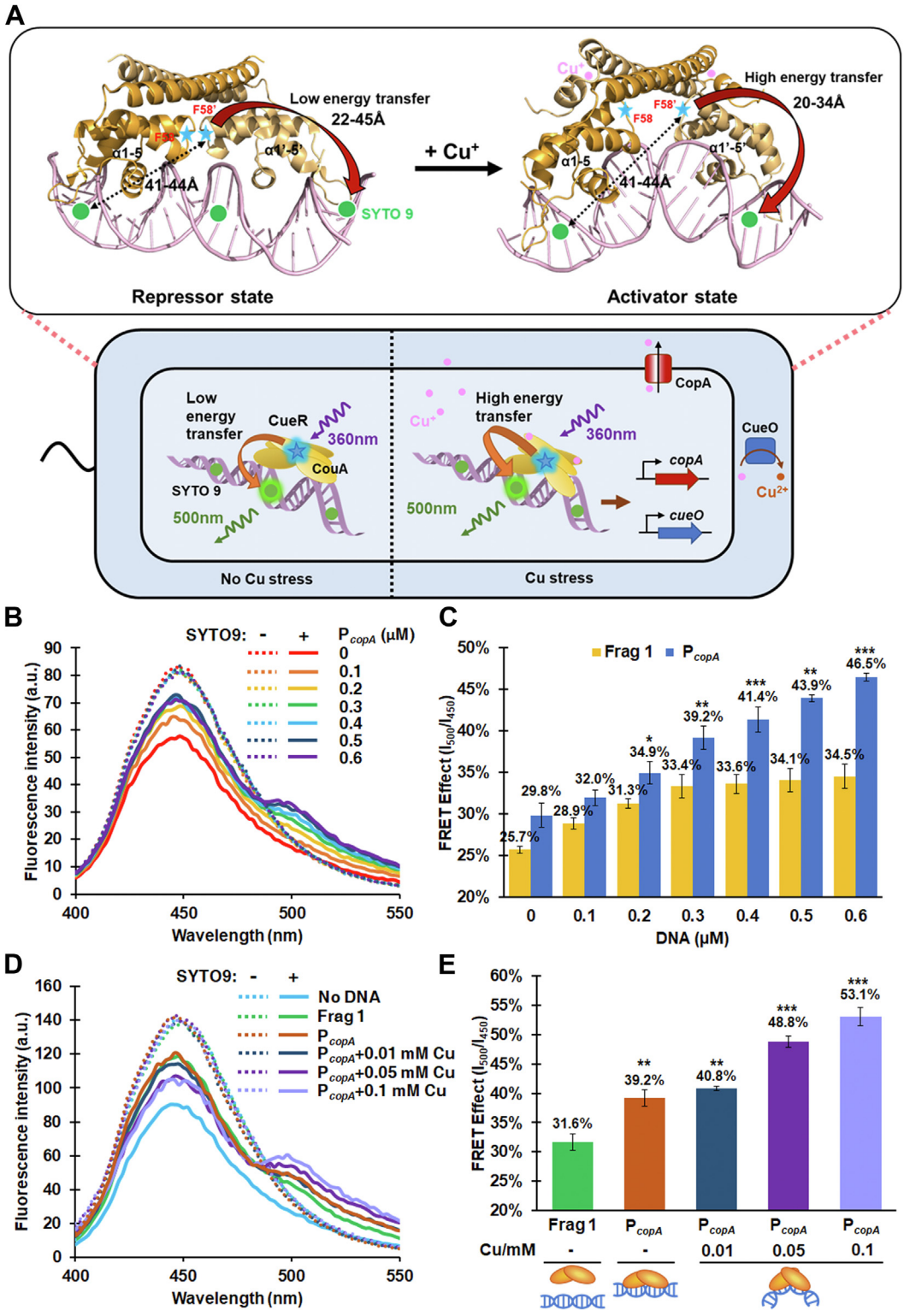

Figure 1. Schematic diagram of the intermolecular FRET-based TF–promoter binding assay and verification of the CouA–SYTO 9 FRET pair employing the CueR–promoter binding model. *A*, diagram of the intermolecular FRET-based TF–promoter binding assay. Structures of the CueR–promoter DNA complex in the repressor and activator states are shown. *Ribbon structure* of CueR–DNA complexes was adopted from the crystal structure of *Escherichia coli* CueR bound to the *copA* promoter DNA (Protein Data Bank IDs: 4WLW and 4WLS). CouA incorporation site F58 was shown. Calculated distances between the F58 and SYTO 9 molecule bound to the proximal DNA minor groove or the distal DNA minor groove in the symmetric CueR dimer–promoter DNA complex were shown. FRET enhancement in the activator–promoter binding state (increase in FRET efficiency) is expected. *Blue stars*, CouA (excitation: 360 nm; emission 450 nm); *green spheres*, SYTO 9 (excitation: 483 nm; emission: 503 nm). *B*, fluorescent spectra of 10 μM CueR–F58CouA purified protein mixed with the P_{copA} DNA fragment (0–0.6 μM) in the presence of SYTO 9 (7.5 μM). *C*, FRET effect (reflected by intensity ratio of 500 to 450 nm) of the CouA–SYTO 9 pair. *D*, fluorescence spectra of purified CueR–F58CouA incubated with a random DNA fragment (frag 1), P_{copA}, or P_{copA} and a series concentration of Cu^+ (0–0.1 mM) in the presence or the absence of SYTO 9. *E*, FRET effect of the CouA–SYTO 9 pair in the assay mixtures. P_{copA}, DNA fragment of promoter region of *copA* gene; Frag 1, random DNA fragment corresponding to +1 - +142 bp in the coding region of *cueR*. Data are the mean of three biological replicates and expressed as mean ± SD. $^*p < 0.05$; $^{**}p < 0.01$; and $^{***}p < 0.001$ (based on Student's *t* test). See also Figs. S1–S3. TF, transcription factor.

is composed of four α-helixes and connected to a two-turn C-terminal α-helix by a hinge loop and a long dimerization helix (35). It was shown that CueR binds to its target promoters as a repressor in the absence of the inducing signal Cu (35). Upon being bound by Cu(I), CueR undergoes a conformational change and is switched to a transcription activator, resulting in a twist of the bound DNA by tightly clamping the α2 and a loop wing of the DBDs, that is, R18, R31, and R37, into DNA major grooves (Fig. 1*A*) (35). Based on this structural information, we chose F58, which is located at the loop region between the helix α3 and helix α4 for CouA incorporation (Fig. 1*A*). The calculated distance between the selected site to the two closest DNA minor grooves, which should be bound by the SYTO 9 dye, is ∼22 and 45 Å, respectively. These distances are within the calculated distance range (25–75 Å) for FRET occurrence based on the theoretical Förster radius of the CouA–SYTO 9 pair (52.5 Å) (Fig. S1).

The genetic code encoding F58 in CueR was mutated to the amber codon TAG. In the presence of the previously optimized orthogonal tRNA–tRNA acetyltransferase MjtRNA–MjTyrRS (26) and the supplement of 1 mM CouA (Fig. S2*A*), a protein band (16.2 kDa) corresponding to CueR–F58CouA-His_6 was detected by fluorescent SDS-PAGE (Fig. S2*B*). The protein was subsequently purified and subjected to LC–MS/MS analysis. Site-specific incorporation of CouA in CueR by replacing F58 was verified by the expected mass of y26 and b4–b15 peptides with a 174.15 Da addition relative to the corresponding peptides derived from the WT CueR (Fig. S2*C*).

FRET effect between CueR–F58CouA and SYTO 9-labeled P_{copA} reliably reports the CueR–P_{copA} binding

We next examined the occurrence of FRET and its degree effected by the binding of purified CueR–F58CouA with the 200-bp DNA fragment of P_{copA} stained with SYTO 9 *in vitro*. Emission spectra of the CueR–F58CouA protein, CueR–F58CouA with the P_{copA} DNA fragment, and CueR–F58CouA with the free SYTO 9 were first recorded. Comparing with the spectra of CueR–F58CouA alone (*red dash line*, Fig. 1*B*) and CueR–F58CouA mixed with varying amounts of P_{copA} (*dash lines*, Fig. 1*B*), which exhibit the characteristic bright fluorescence of CouA peaked at 450 nm, addition of free SYTO 9 caused a slight decrease of the overall fluorescence intensity (*red solid line*, Fig. 1*B*), which was found to be saturated when SYTO 9 concentration is above 5 μM (Fig. S3*A*). Since the decrease of fluorescence intensity at 450 nm was not accompanied by an increase of fluorescence intensity at 500 nm, which is the desired FRET signal for the CouA–SYTO 9 pair, the decrease of CouA emission fluorescence in these control mixtures is mostly because of a fluorescence quenching of CouA by the free SYTO 9 and is not a false-positive FRET. When the protein (10 μM) was mixed with varying amounts of P_{copA} DNA fragment in the presence of SYTO 9 (7.5 μM), a significant fluorescence emission peaked at 500 nm appeared, and the intensity increased in a P_{copA} concentration–dependent manner (Fig. 1, *B* and *C*), indicating the occurrence of FRET between CueR–F58CouA and the SYTO 9-bound P_{copA}, which led to the energy transfer from CouA to SYTO 9. In contrast, supplying a random DNA fragment (Frag 1) only caused a very moderate increase at 500 nm, and the intensity was not increased continuously with the increase of the DNA concentration (Fig. 1*C*), suggesting that the FRET signal observed in the mixture of CueR–F58CouA and P_{copA} was effected by the specific interaction between CouA–F58CouA and the SYTO 9-bound P_{copA}. This result is consistent with the fact that CueR binds to its target promoters as a repressor in the absence of the inducing signal Cu(I). Since the background-level FRET between CueR–F58CouA with a random DNA was saturated when its concentration was above 0.3 μM (Fig. 1*C*), 0.3 μM DNA fragment is applied in the following assays. Next, we supplied the stimulant Cu(I), which is generated by $CuSO_4$ in the presence of ascorbate to the assay mixture. A dose-dependent increase of the FRET signal was observed (Fig. 1, *D* and *E*), indicating a closer proximity and improved alignment between the FRET pairs upon Cu(I) binding to CueR, which is consistent with the clamp of DBD into DNA grooves by the Cu-bound CueR activator as revealed in the crystal structure of the CueR–promoter DNA complex (35). The observed FRET should occur between the CouA58 donor in one CueR protomer with the SYTO 9 acceptor that binds to the proximal minor groove of the pseudopalindrome DNA in the symmetric CueR dimer–DNA complex (Fig. 1*A*) because their distance undergoes a change from 22 to 45 Å in the repressor state to 20 to 34 Å in the activator state, whereas the distance between the same CouA58 and a SYTO 9 molecule bound to the distal DNA minor groove occupied by the other CueR protomer remains largely unchanged (41–44 Å) during the transition process (Fig. 1*A*). These results demonstrated that the FRET occurrence and its degree between CouA and SYTO 9 reliably reports the intricate interaction of CueR with its targeting promoter DNA in response to the presence and strength of the inducing signal of the regulatory system.

Whole-cell FRET between $CueR_{CouA}$ and $promoter_{SYTO\ 9}$ monitors CueR–promoter interaction in vivo

We next employed the FRET pair to monitor the TF–promoter interactions in living *E. coli*. To achieve this, we first optimized the condition for CouA incorporation in *E. coli* cells such that CouA is incorporated into CueR, but the protein is not overexpressed to artificially shift or saturate the TF–promoter binding. We carried out CouA incorporation and protein expression under a mild condition (0.5 mM IPTG, 0.4% arabinose, and 1 mM CouA for 4 h at 37 °C) compared with that for overexpression and purification of CueR–F58CouA. The expression level of CueR–F58CouA protein in the cell cultured under this condition was estimated to be ∼113 μg/ml (Fig. S4*A*) (37). Using promoter-*lacZ* fusion of the CueR-regulated gene *cueO* (P_{cueO}-*lacZ*) as a reporter, it was shown that the level of CueR–F58CouA produced under this condition did not lead to nonspecific binding of CueR to its targeting promoter and activation of the *cueO* gene (Fig. S4*B*).

Fluorescent SDS-PAGE (Fig. S2*B*) and fluorescent microscopy (Fig. S5*A*) further confirmed the expression of CueR–F58CouA and the bright fluorescence of the resulting cell suspension. To determine the concentration of SYTO 9 to be applied in the whole-cell FRET assay, we first examined the background fluorescence intensity of *E. coli* BL21 cell suspension stained with a series concentration (0.5–20 μM) of SYTO 9. Although a concentration-dependent increase of the fluorescence intensity at 500 nm was observed, the signal intensity (0–20 a.u.) was moderate (Fig. S3*B*). Based on this and studies of McGoverin *et al.* (38), which suggested that micromolar (1 μM) SYTO 9 is suitable for general application of the dye in bacteria, the same SYTO 9 concentration (7.5 μM) as applied in the *in vitro* assay was selected for the *in vivo* assay. Staining of cell suspension with this concentration of SYTO 9 yielded the desired bright green fluorescence (Fig. S5*A*), confirming the applicability of both fluorophores SYTO 9 and CouA in live bacteria.

A whole-cell FRET measurement to monitor *in vivo* TF–promoter binding was subsequently established. About 0.1 mM $CuSO_4$ was added in the cell culture during CouA incorporation and CueR–F58CouA expression to activate CueR-mediated transcription regulation. Following incubation with SYTO 9 for 15 min in the dark, the whole-cell suspension was directly subjected to emission fluorescence spectrum recording (Fig. 2*A*). Comparing with the spectrum without the Cu stress (*cyan line*, Fig. 2*B*), which exhibited a background-level FRET (50.8%) (Fig. 2*F*), an obvious FRET enhancement with a quantified FRET effect of 61.7% was observed in the cell treated with 0.1 mM Cu (*purple line*, Fig. 2*B*), suggesting that the CouA–SYTO 9 FRET pair is applicable to report the binding of CueR with its promoter in live *E. coli* cells in response to the Cu stress. To confirm that the observed FRET effect and its enhancement was elicited by the specific binding of CueR with its target promoters (P_{copA} and P_{cueO}) in *E. coli* cells, we mutated the key arginine residues R18 and R37 located at the loop wing of the promoter-binding domain of CueR, which are essential for DNA clamping (33), and conducted the assays employing *E. coli* cells expressing CueR–F58CouA–R18A and CueR–F58CouA–R37A, respectively. No FRET enhancement was observed when cells expressing either of the mutant proteins were treated by Cu compared with that without Cu treatment (Fig. 2, *C* and *D*). Quantitation of the degree of FRET confirmed the insignificant FRET changes for CueR–F58CouA–R18A and CueR–F58CouA–R37A as opposed to that (10.9%) for the CueR–F58CouA (Fig. 2*F*). To further confirm the specificity of the FRET signals observed, we also conducted the assay in a mutant strain in which the only two targeting promoters of CueR in the *E. coli* genome, P_{copA} and P_{cueO}, were deleted from the *E. coli* BL21 genome, that is, BL21 (DE3) $\Delta P_{copA}\Delta P_{cueO}$. Whole-cell FRET assay in this mutant showed that deletion of the targeting promoters completely abolished the FRET effect between $CueR_{F58CouA}$ and promoter $DNA_{SYTO\ 9}$ (Fig. 2, *E* and *F*). These results demonstrated the specificity and sensitivity of the intermolecular FRET-based whole-cell TF–promoter binding assay we developed.

To establish the CouA incorporation locations applicable for the intermolecular FRET-based TF–promoter binding assay, we incorporated CouA into several additional locations (Fig. 3*A*) and constructed the following variants: CueR–T27CouA, CueR–Y39CouA, and CueR–Q74CouA, in which CouA was incorporated into the loop region between the α2 and α3 in the DBD (T27CouA and Y39CouA) and the loop region between α4 in the DBD and the α5 dimerization helix (Q74CouA). The calculated distances between these sites and the closest central minor grooves, which should be bound by SYTO 9, are 26, 30, and 36 Å, respectively. Whole-cell assay showed that an enhancement of FRET upon Cu treatment was also observed in cells expressing CueR–T27CouA (Fig. 3, *B* and *E*) and CueR–Y39CouA (Fig. 3, *C* and *E*), but not in cells expressing CueR–Q74CouA (Fig. 3, *D* and *E*), suggesting that the donor fluorophore (CouA) can be incorporated into multiple locations in the DBD, especially the loop regions between α helices, but not the distal dimerization domain for the FRET-based assay. Notably, we also constructed a plasmid encoding the CueR–P73CouA variant, but the protein was not successfully expressed despite its close proximity to Q74. This result suggested that certain residues, such as proline, are not tolerant to replacement by CouA.

The CouA–SYTO 9 FRET pair reports the intricate CueR–promoter interaction elicited by transient signals in living cells and novel signals that activate CueR

Next, we applied the assay to detect the activation or inactivation of the CueR regulatory system by indirect or intermediate stimulant. Zinc (Zn) was indicated to inactivate CueR indirectly through transiently elevating intracellular iron (Fe) (39). To verify this regulatory circuit, we examined FRET occurrence and its degree in *E. coli* cells expressing CueR–F58CouA and stained with SYTO 9 in the presence of Zn, which should suppress the CueR–promoter interaction, and Zn in combination with the Fe chelator 2,2′-dipyridyl, which should restore the CueR–promoter interaction. As shown in Figure 3*F*, while a significant FRET was observed in the presence of Cu, addition of Zn abolished the FRET effect. Further supplementing 2,2′-dipyridyl restored the FRET effect, confirming the regulatory circuit of Zn–Fe–CueR (39).

We also employed the FRET-based assay to explore novel signals that can activate CueR. We found that supplementing 0.02 mM manganese (Mn) (40) also resulted in an enhancement of FRET (Fig. 3*G*) with a calculated FRET change of 6.3% (Fig. 3*H*), whereas nickel (Ni) (0.02 mM) did not elicit a FRET enhancement in cells expressing CueR–F58CouA, suggesting that Mn may also serve as a signal to activate CueR. To verify this finding, we performed β-galactosidase activity assay to examine the transcription of P_{copA}-*lacZ* and P_{cueO}-*lacZ* in the presence of the same concentration of these metals, which do not inhibit the growth of *E. coli* cells. β-galactosidase activity assay showed that Mn supplement indeed activated transcription of the P_{copA}-*lacZ* and P_{cueO}-*lacZ* fusions that are controlled by CueR, whereas Ni supplement did not (Fig. 3*I*). This result verified that the whole-cell intermolecular

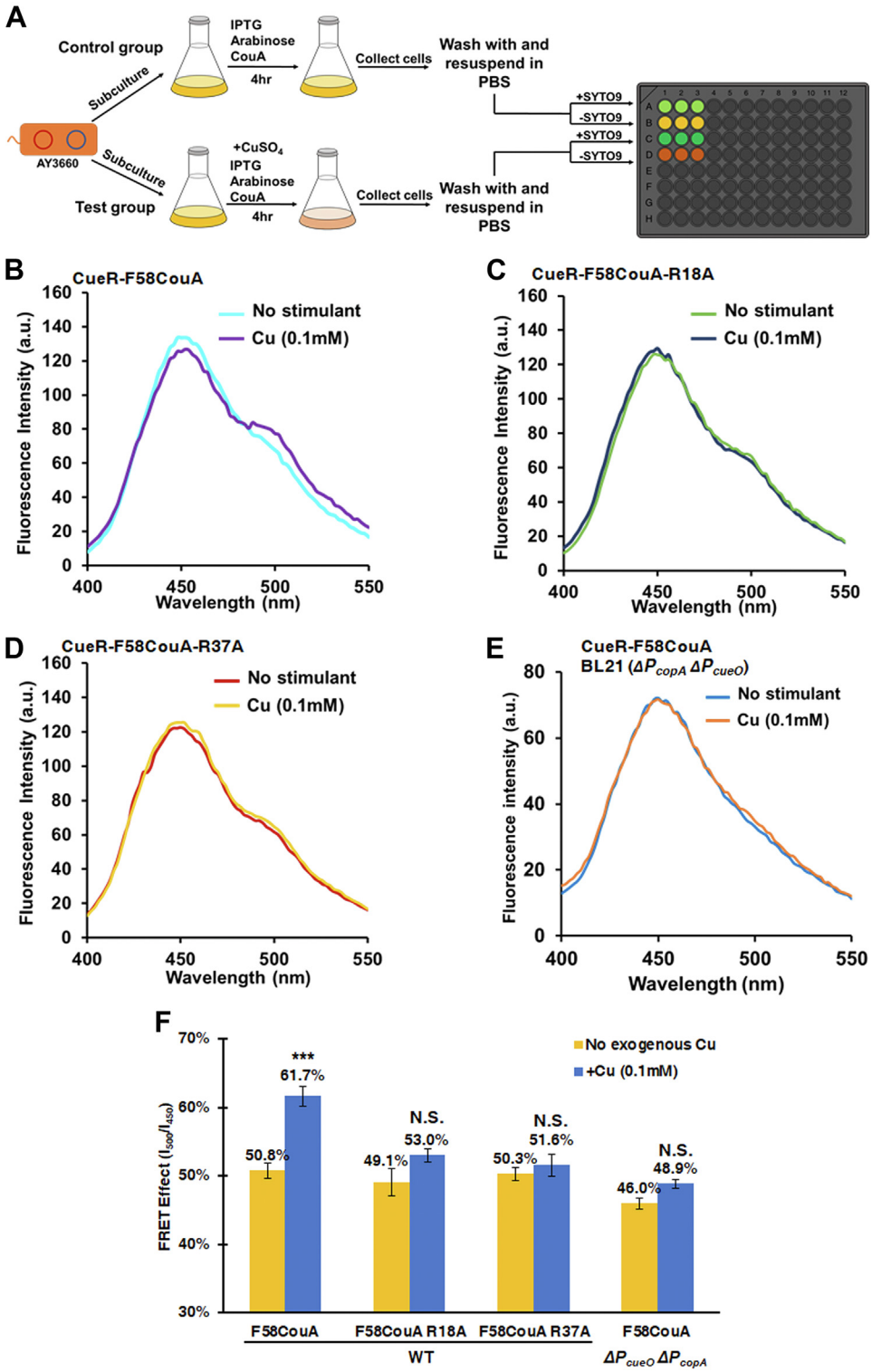

Figure 2. The intermolecular FRET-based TF–promoter binding assay detects the specific interaction of CueR with its regulated promoters in living *Escherichia coli*. *A*, sample preparation workflow for the FRET-based CueR–promoter binding assay *in vivo*. About 0.1 mM $CuSO_4$ was added to the test group to activate CueR. Cell suspension was incubated in the dark for 15 min before being subjected to fluorescence recording. *B–D*, fluorescence spectra of BL21 (DE3) cells expressing CueR–F58CouA (AY3660) (*B*), or CueR–F58CouA–R18A (AY3793) (*C*), or CueR–F58CouA–R37A (AY3794) (*D*), under noninducing condition and in the presence of 0.1 mM $CuSO_4$. All data are normalized against the conditions of no SYTO 9 addition. *E*, fluorescence spectrum of BL21 (DE3)- ΔP_{copA} ΔP_{cueO} cells (AY7038) expressing CueR–F58CouA under noninducing condition (*blue*) and in the presence of 0.1 mM $CuSO_4$ (*orange*). *F*, FRET effect of the CouA–SYTO 9 pair in the designated assay mixtures. Data are the mean of three biological replicates and expressed as mean ± SD. *$p < 0.05$; **$p < 0.01$; ***$p < 0.001$; NS, not significant relative to the no-metal treatment (based on Student's *t* test). See also Figs. S3–S5. TF, transcription factor.

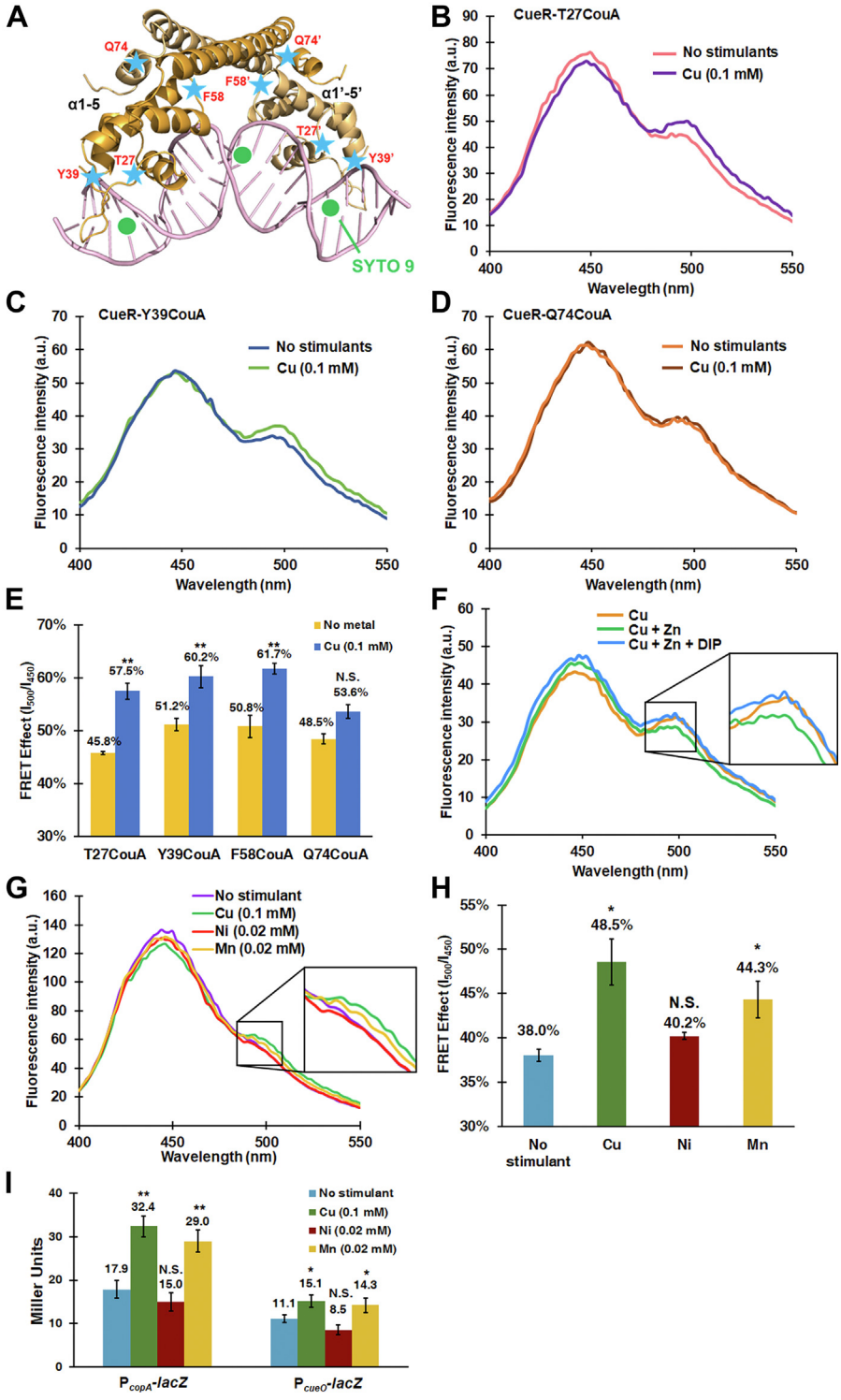

Figure 3. Whole-cell intermolecular FRET-based TF–promoter binding assay reports the intricate interactions of CueR–promoters in living cells. *A*, diagram showing the locations of CouA incorporation sites tested. CueR is shown in its active state (Protein Data Bank ID: 4WLW). *Blue stars* represents CouA, and *green spheres* represent SYTO 9. *B–D*, fluorescence spectra of BL21 (DE3) cells expressing CueR–T27CouA (*B*), or CueR–Y39CouA (*C*), or CueR–Q74CouA (*D*) in the presence or the absence of 0.1 mM $CuSO_4$. *E*, FRET effect of the CouA–SYTO 9 pair in the designated cell suspensions. *F* and *G*, fluorescence spectra of BL21 (DE3) cells expressing CueR–F58CouA in the presence of 0.1 mM $CuSO_4$ (*orange*), 0.1 mM $CuSO_4$ and 0.1 mM $ZnCl_2$ (*green*), and 0.1 mM $CuSO_4$, 0.1 mM $ZnCl_2$, and 0.2 mM DIP (*blue*) (*F*), 0.1 mM $CuSO_4$ (*green*), 0.02 mM $NiCl_2$ (*red*), and 0.02 mM $MnCl_2$ (*yellow*) (*G*). All data are normalized against the conditions without SYTO 9 addition. *H*, FRET effect of the CouA–SYTO 9 pair in the designated cell suspensions. *I*, β-galactosidase activities of P_{copA}-*lacZ* and P_{cueO}-*lacZ* transcription fusions in the presence of Cu, Mn, and Ni. Data are the mean of three biological replicates and expressed as mean ± SD. $^*p < 0.05$; $^{**}p < 0.01$; $^{***}p < 0.001$, and NS, not significant relative to no-metal treatment (based on Student's *t* test). See also Fig. S7. DIP, 2,2′-dipyridyl; TF, transcription factor.

FRET-based assay we established is applicable to report TF–promoter interaction occurred in a complex regulatory circuit induced by indirect stimulants and can be employed to identify novel signals and conditions that modulate the regulatory system of interest.

The intermolecular FRET-based TF–promoter binding assay monitors the signal transduction of two-component regulatory systems

We next extended the methodology to another class of important gene regulatory system in bacteria: the TCS. TCS is composed of a membrane-bound histidine kinase (HK) that senses the extracellular signals and a cognate response regulator (RR) that regulates gene transcription in response to signals perceived by the HK. We chose the BasSR TCS to test the application of the whole-cell intermolecular FRET-based TF–promoter binding assay. In this TCS, BasS is the HK that senses high iron (Fe^{3+}) level and phosphorylates the cognate RR BasR (Fig. 4*A*) (41). Phosphorylated BasR binds to the promoters of its target genes *ugd*, *eptA*, and *arn* operon, which encode enzymes that modify lipid A on the outer membrane of Gram-negative bacteria, and activates their transcription (Fig. 4*A*) (42).

To monitor the activation of BasR in response to Fe^{3+} stress and interaction of BasR with its target promoters *in vivo*, we set out to incorporate CouA into the DBD of the BasR protein. The crystal structure of BasR is not available. To determine the CouA incorporation sites, we employed I-TASSER server (https://zhanglab.ccmb.med.umich.edu/I-TASSER/) to simulate the 3D structure of BasR using the crystal structure of its homolog, *Klebsiella pneumoniae* PmrA (Protein Data Bank [PDB] ID: 4S05), as the template (43–45). Two domains were identified in the predicted structure, the receiver domain (1–121 amino acids) and the DBD (125–219 amino acids). The DBD encompasses three α-helices (α6–α8) and two β-sheets (β2 and β3). Four potential CouA incorporation sites were selected, G137 (located in β2), E146 (located in a loop region between β2 and α6), S167 (located in a loop region between α6 and α7), and D182 (located in a loop region between α7 and α8) (Fig. 4*B*). They display a calculated distance of 26, 28, 24, and 22 Å, respectively, to the closest DNA minor grooves. Herein, we replaced the T7 promoter in pET28a to pBAD and conducted the assay in the *E. coli* reference strain MG1655 (46). Expression of BasR and CouA incorporation was carried out in the presence of 0.9% arabinose. Expression of the resulting CouA-incorporated proteins (BasR–S137CouA as an example) was monitored by Western blot (Fig. S4*C*) and verified by fluorescent SDS-PAGE (Fig. S2*B*), fluorescent microscopy (Fig. S5*B*), and LC–MS/MS (Fig. S2*D*).

To monitor the activation of the BasSR in response to Fe^{3+} stress, *E. coli* MG1655 cells expressing CouA-incorporated BasR was treated with 0.5 mM Fe^{3+} in the MOPS medium for 1 h before being stained with SYTO 9 and subjected to emission fluorescence recording. The whole-cell suspension contained a similar ratio of the donor fusion and acceptor stain as employed in the case of CueR–promoter assay, that is, cells with an absorbance unit (a.u.) of 10 stained with 7.5 μM SYTO 9. Emission fluorescence recording showed that upon Fe^{3+} treatment, a statistically significant FRET enhancement relative to the nontreatment control was observed in all these cells, that is, BasR–G137CouA, BasR–E146CouA, BasR–S167CouA, and BasR–D182CouA (Fig. 4, *C*–*F*). The degree of FRET enhancement was calculated to be 6.0, 9.2, 6.9, and 6.9%, respectively (Fig. 4*G*). To verify that the FRET assay indeed reported the activation of BasR and its binding to the target promoters, we examined the phosphorylation of BasR protein under this culture and assay condition using Phos-tag SDS-PAGE. It was shown that a significant portion of BasR was phosphorylated in the presence of 0.5 mM Fe^{3+}, confirming that the intermolecular FRET-based assay we developed is applicable to monitor the activation of the TCS *in vivo*. Furthermore, the fact that incorporation of CouA into all four selected sites resulted in the desired FRET enhancement upon stimulation and that these CouA incorporation sites were determined based on the simulated 3D structure of BasR suggested that the assay system we developed is robust to monitor the diverse signal transduction systems.

Whole-cell FRET measurement monitors the activation of PhoPQ TCS in response to different stimulants

We next expanded the assay to the PhoPQ regulatory system, which is one of the most important TCS in enterobacteria that regulates the virulence and antibiotic resistance in response to the environment of their mammalian hosts, such as low divalent cations, low pH, antimicrobial peptides, and osmotic upshift (47–53). In this TCS, PhoQ is the HK that phosphorylates and activates the RR PhoP upon perceiving stimulating signals. Phosphorylated and activated PhoP then binds to the target promoters to regulate gene transcription (Fig. 5*A*). Since the crystal structure of *E. coli* PhoP is not available, we simulated its 3D structure using the crystal structure of *Mycobacterium tuberculosis* PhoP–DNA complex (PDB ID: 5ED4) as the template. Two domains were shown in the simulated structure, the receiver domain (1–123 amino acids) and the DBD (123–223 amino acids). The DBD encompasses three α helixes (α6–α8) and two β-sheets (β2 and β3). We selected three potential sites in the DBD for CouA incorporation, S137 (located in β2), D145 (located at the loop region between β2 and α6), and A182 (located at the loop region between α7 and α8) (Fig. 5*B*). The calculated distances of D145, S137, and A182 to the closest DNA minor groove are approximately 30, 25, and 20 Å, respectively. Plasmids encoding the three proteins PhoP–S137CouA, PhoP–D145CouA, and PhoP–A182CouA were successfully constructed. Fluorescent SDS-PAGE (Fig. S2*B*), fluorescent microscopy (Fig. S5*C*), and LC–MS/MS (Fig. S2*E*) analysis confirmed the expression of these proteins (PhoP–A182CouA as an example) and their fluorescence in *E. coli* cells.

We first conducted the whole-cell FRET assay to monitor the activation of the regulatory system under the condition of Mg^{2+} depletion. About 10 mM Mg^{2+} was added in the cell suspension to ensure that PhoPQ is fully inactivated prior to applying the

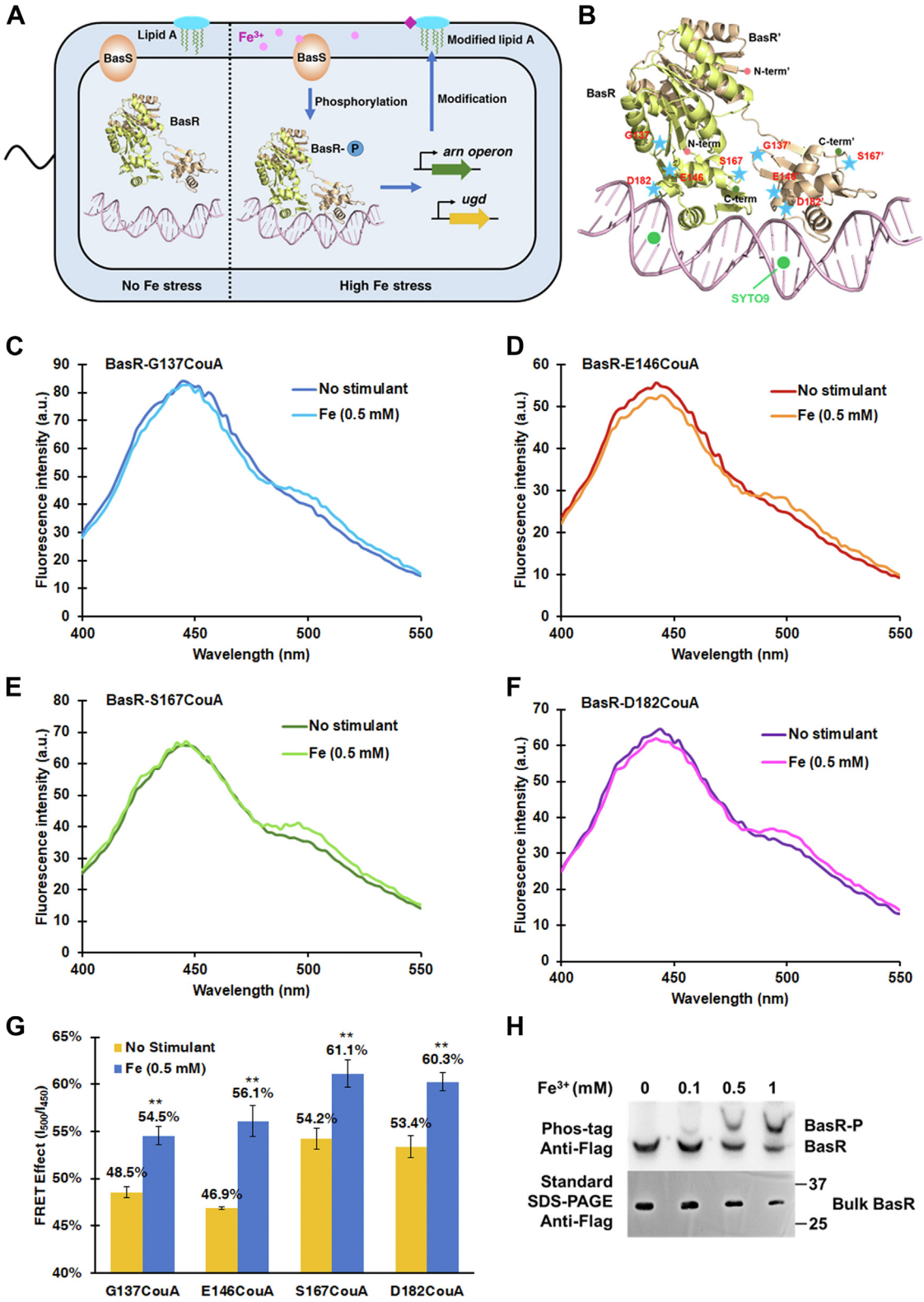

Figure 4. The intermolecular FRET-based TF–promoter binding assay system monitors activities of the two-component system (TCS) BasSR *in vivo*. *A*, diagram showing the signal transduction of the BasSR TCS. *B*, diagram showing the locations of CouA incorporation sites in BasR tested in this study. BasR is shown in its active state. *Blue stars* represent CouA, and *green spheres* represent SYTO 9. Ribbon structure of BasR was simulated using the I-TASSER server. DNA fragment was adopted from crystal structure of *Klebsiella pneumoniae* PmrA (Protein Data Bank ID: 4S05). *C–F*, fluorescence spectra of MG1655 cells expressing BasR–G137CouA (*C*), BasR–E146CouA (*D*), BasR–S167CouA (*E*), and BasR–D182CouA (*F*) in the presence or the absence of 0.5 mM Fe^{3+}. *G*, FRET effect of the CouA–SYTO 9 pair in the designated assay mixtures. *H*, phosphorylation of BasR in the presence of a series of $FeCl_3$ detected by Phos-tag SDS-PAGE. Bands corresponding to phosphorylated (BasR-P) and unphosphorylated BasR (BasR) are indicated. Data are the mean of three biological replicates and expressed as mean ± SD. *$p < 0.05$; **$p < 0.01$; ***$p < 0.001$; NS, not significant relative to no-metal treatment (based on Student's *t* test). See also Figs S2, S4, S5, and S7. TF, transcription factor.

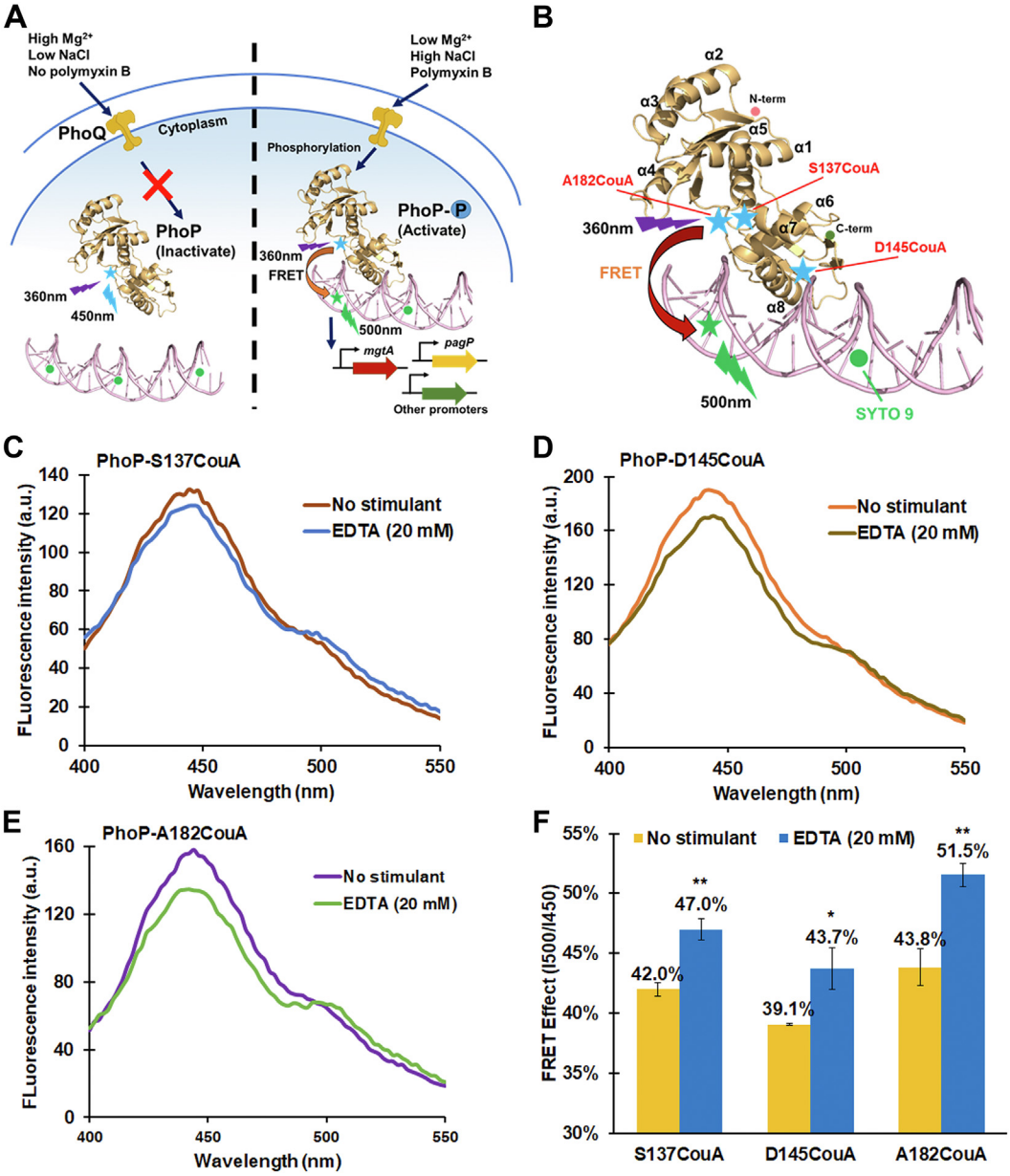

Figure 5. The intermolecular FRET-based TF–promoter binding assay monitors the activities of the PhoPQ TCS. *A*, diagram of the intermolecular FRET-based PhoP–promoter binding assay. *Blue stars*, CouA (excitation: 360 nm; emission: 450 nm); *green spheres*, SYTO 9 (excitation: 483 nm; emission: 503 nm). *B*, diagram showing the locations of CouA incorporation sites in PhoP. PhoP is shown in its active state. *Blue stars* represent CouA, and *green spheres* represent SYTO 9. *Ribbon structure* of PhoP was simulated using the I-TASSER server. DNA fragment was adopted from crystal structure of *Mycobacterium tuberculosis* PhoP–DNA complex (Protein Data Bank ID: 5ED4). *C–E*, fluorescence spectra of BL21 (DE3) cells expressing PhoP–S137CouA (*C*), or PhoP–D145CouA (*D*), or PhoP–A182CouA (*E*) and stained with SYTO 9 in the presence or the absence of 20 mM EDTA. *F*, FRET effect of the CouA–SYTO 9 pair in the corresponding assay mixtures. Data are the mean of three biological replicates and expressed as mean ± SD. *$p < 0.05$; **$p < 0.01$; ***$p < 0.001$; NS, not significant relative to no EDTA treatment (based on Student's *t* test). See also Figs. S5 and S7. TCS, two-component system; TF, transcription factor.

stimulants as reported by Bader *et al.* (50). Depletion of Mg^{2+} was initiated subsequently by supplying 20 mM EDTA following a previous description (53). An enhancement of FRET was observed in all three assay mixtures relative to the no-EDTA control (Fig. 5, *C–E*). Among them, PhoP–A182CouA displayed the greatest degree of FRET enhancement (7.7%) (Fig. 5*F*), consistent with the closest calculated distance between this site with the DNA minor groove among the three selected sites in the simulated structure.

Next, we employed the assay to detect the activation of the PhoPQ system by the cationic antimicrobial agent polymyxin B. Herein, the stimulant was applied to the cell suspension with a physiological level of Mg^{2+} (1 mM). We monitored time course of the FRET effected by PhoP–A182CouA and target promoters bound by SYTO 9 following applying varying concentrations of polymyxin B. Dose-dependent FRET enhancement was observed at all three time courses: 10, 20, and 30 min (Fig. 6, *A* and *C*). The FRET enhancement maintained during the entire signal recording process (30 min), suggesting a strong and continuous activation of the PhoPQ TCS by polymyxin B. We also monitored the FRET occurrence effected by EDTA treatment in the same

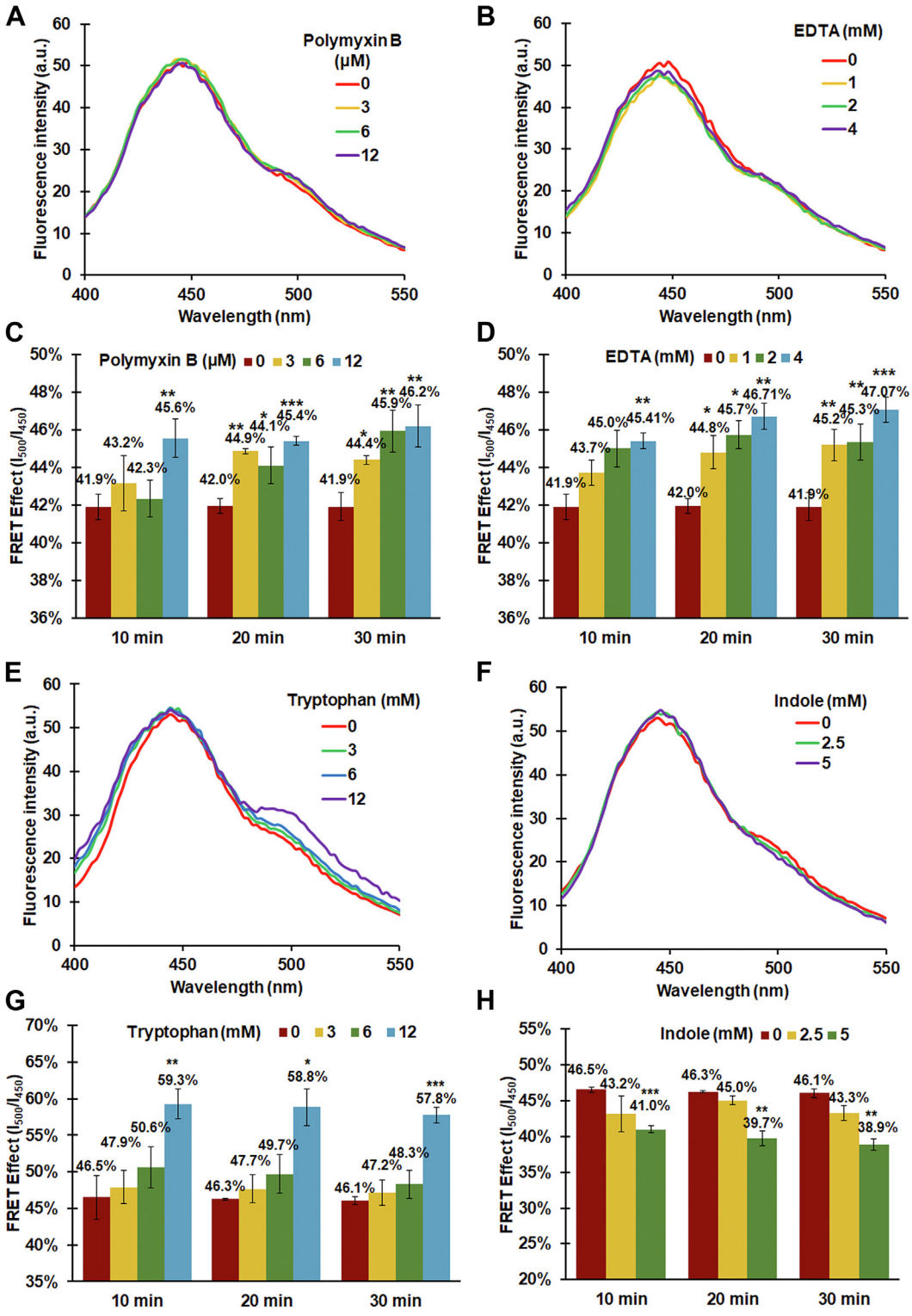

Figure 6. Intermolecular FRET-based assay system monitors PhoP activities in response to different stimulants and identifies novel modulators of the PhoPQ system. *A*, *B*, *E*, and *F*, fluorescence spectra of BL21 (DE3) cells expressing PhoP–A182CouA (AY3709) treated by polymyxin B (*A*), EDTA (*B*), tryptophan (*C*), or indole (*F*). *C*, *D*, *G*, and *H*, FRET effect of the CouA–SYTO 9 pair in the designated assay mixtures. Data are the mean of three biological replicates and expressed as mean ± SD. *$p < 0.05$; **$p < 0.01$; and ***$p < 0.001$ (based on Student's *t* test). See also Fig. S6.

cell suspension, that is, physiological level of Mg^{2+}, and observed a similar pattern for FRET occurrence, and its degree and dynamics (Fig. 6, *B* and *D*). This result suggested that PhoPQ exerts similar signal perception and regulatory response in response to these two types of stimulants, and polymyxin B activates the PhoPQ system by competing the Mg^{2+}-binding site in the sensor domain of PhoP as proposed by Bader *et al.* (50).

Whole-cell FRET monitoring of TF–promoter interactions

Whole-cell FRET-based TF–promoter binding assay enables identification of novel modulators of the PhoPQ TCS

The development of genome assembly, genetics, and high-throughput gene expression analysis has allowed identification of a large number of TCSs in bacterial genomes (54–56). However, a major bottleneck in understanding these signal transduction systems is the lack of information on the environmental signals and physiological conditions that trigger their activation (57, 58). In addition to reporting the *in situ* TF–promoter interaction in response to know stimulants of a signal transduction system, the FRET-based *in vivo* TF–promoter binding assay we developed can be employed to identify modulators of a regulatory system as demonstrated in the case of aforementioned CueR. To further expand the applications, we explored novel signals that modulate the PhoPQ TCS. Several previous DNA microarray studies indicated that a class of indole and its derivatives, such as indole-3-acetic acid (IAA) and tryptophan, and the aminoglycoside antibiotic gentamycin altered expression of PhoP in *E. coli* cells (59–62). It was indicated that treatment with IAA, gentamycin, and tryptophan increased the expression of PhoP, whereas indole treatment reduced its expression. To verify whether these signals indeed modulate the PhoPQ system, we treated *E. coli* cells expressing PhoP–A182CouA with these chemicals and monitored the FRET signal. As shown in Figure 6, *E* and *G*, treatment with 12 mM tryptophan resulted in an enhancement of FRET (46–58%). Indole treatment, on the other hand, caused a slight reduction of FRET (Fig. 6, *F* and *H*). Growth curve analysis indicated that 2.5 mM or above indole caused a significant reduction on the growth rate of *E. coli* (Fig. S6), suggesting that the reduction on FRET upon indole treatment may be due to perturbation on the growth of *E. coli* cells. In contrast, IAA and gentamycin treatment did not elicit a FRET effect despite a broad range of concentrations and treatment time were tested (Fig. S6). These studies demonstrated that the FRET-based assay we developed is applicable to identify and verify modulators of TCSs.

FRET-based TF–promoter assay monitors the activation of the PhoPQ system *in* E. coli *cells colonized in the* C. elegans *gut*

Next, we expanded the assay system to monitor the activation of a signal transduction system and TF activities in bacteria colonized in an animal host using *C. elegans* as a paradigm. *C. elegans* is a model organism widely employed to study bacteria–host interactions including that of both pathogens and microbiome with their animal hosts (63–65) because of its invariant cell lineage, simple body structure, and short life cycle (66, 67). Studies have indicated that global and specific TFs such as the TCS FsrAB in *Enterococcus faecalis* and the global TF GacA in *Pseudomonas aeruginosa* play an important role in their pathogenesis in the *C. elegans* infection model (63). Toward a proof of concept of the application of the FRET-based TF–promoter binding assay for studying gene regulation in the bacteria–host interface, we tested the application of the FRET-based assay to report the activation of PhoP in *E. coli* colonized in the *C. elegans* gut as PhoPQ serves as the primary regulatory system during the adaptation of enterobacteria to their host environments (68–70). We fed the *C. elegans* L4 stage larva with *E. coli* BL21 cells expressing PhoP–A182CouA (AY3706) and stained with SYTO 9 (Fig. 7*A*). *C. elegans phm-2(-)* mutant animals (DA597) were used in the experiment because they have a dysfunctional grinder (71), allowing the observation of intact *E. coli* in *C. elegans* gut. *C. elegans* fed with the *E. coli* OP50 served as a control (Fig. 7*B*). The expected blue fluorescence (420–480 nm) (Fig. 7*C*, *upper left panel*) and green fluorescence (490–600 nm) (Fig. 7*C*, *upper right panel*), which corresponds to the emission of CouA and SYTO 9, respectively, was observed in the *C. elegans* intestinal tract when the animals were excited at 405 and 488 nm, respectively. Particularly, the fluorescence in the gut was shown as small puncta rather than being diffused, indicating the presence of intact *E. coli* cells emitting fluorescence of PhoP–A182CouA and SYTO 9 bound with DNA in the *C. elegans* gut.

To examine whether PhoPQ system is activated to bind its target promoters and regulate gene expression in the *C. elegans* gut, we excited the *C. elegans* at 405 nm and recorded the green fluorescence emitted by SYTO 9 bound with DNA in the *C. elegans* intestinal lumen (490–600 nm) (Fig. 7*C*, *lower left panel*), that is, FRET effect. FRET signals were recorded in several focal points in the gut lumen, indicating the binding of PhoP–A182CouA with SYTO 9-stained targeting promoters in these *E. coli* cells (Fig. 7*C*, *lower left panel*). Colocalization of the signals corresponding to the emission fluorescence of CouA and SYTO 9 with that of FRET further confirmed this result (Fig. 7*D*). Hence, the method we developed is applicable to examine TF activities at the bacteria–host interface.

FRET-based TF–promoter assay is applicable for single-cell analysis

To further expand the application scopes of the FRET-based TF–promoter assay, we also conducted FRET analysis to examine TF activity at single-cell level. *E. coli* MG1655 expressing BasR–G137CouA was subjected to excessive Fe^{3+} (0.5 mM) treatment for 1 h. Treated and untreated bacteria cells were then deposited onto an agarose pad and subjected to confocal microscopy analysis. As shown in Figure 8*A*, cells treated with 0.5 mM Fe^{3+} displayed brighter emission fluorescence at 500 nm (emission fluorescence of SYTO 9) than the untreated cells upon excitation at 405 nm (the excitation wavelength of CouA). We quantified the FRET effect in single cells by measuring fluorescence intensity in the CouA channel (*blue*) and FRET channel (*green*) along the long axis of 20 cells in each of the samples (72). As shown in Figure 8*B*, a significant FRET effect was observed in cells treated with 0.5 mM Fe^{3+}, which is consistent with the result obtained by spectroscopy analysis of cell culture shown in Figure 4*G*. Hence, the FRET-based TF–promoter binding assay we developed can be conducted at single-cell level and employed for single-cell analysis.

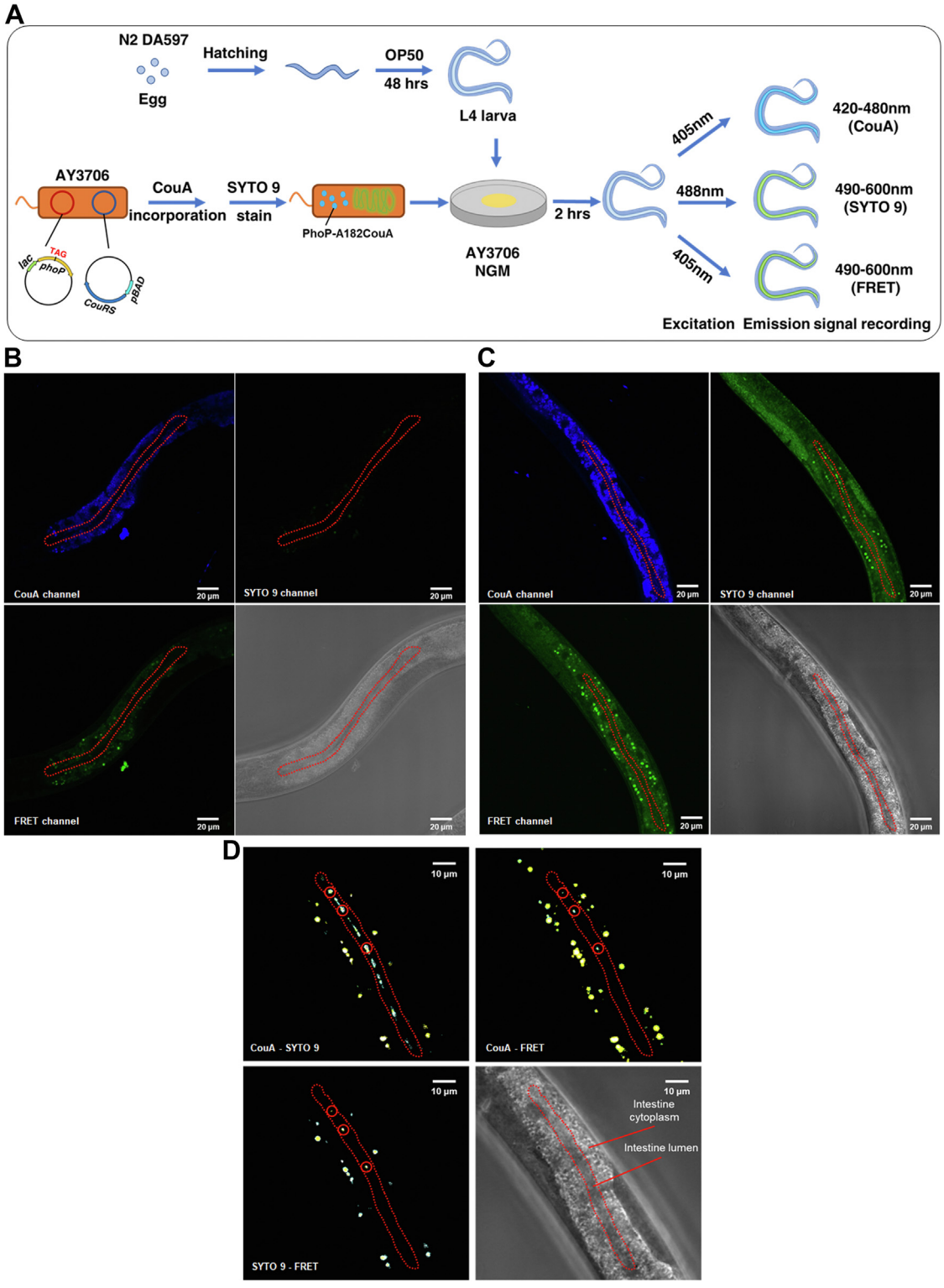

Figure 7. FRET measurement reports the PhoP–promoter activity in *Escherichia coli* colonized in the *Caenorhabditis elegans* gut. *A*, workflow of the intermolecular FRET-based assay in the *C. elegans* colonization model. *B* and *C*, fluorescence of *C. elegans* fed with OP50 (*B*) or BL21 (DE3) cells expressing PhoP–A182CouA (AY3709) (*C*) examined by confocal fluorescent microscope. *Upper left*, CouA emission fluorescence recorded in the range of 420 to 480 nm upon excitation at 405 nm. *Upper right*, SYTO 9 emission fluorescence recorded in the range of 490 to 600 nm upon excitation at 488 nm. *Lower left*, FRET signal recorded in the range of 490 to 600 nm upon excitation at 405 nm. *Lower right*, differential interference contrast (DIC) image of the *C. elegans* intestine area subjected to fluorescence recording. *D*, colocalization of different fluorescent channels in the intestine area of *C. elegans* in (*C*). *Red circles* indicate the colocalization between the indicated fluorescent channels. *Upper left*, CouA channel and SYTO 9 channel. *Upper right*, CouA channel and FRET channel. *Lower left*, SYTO 9 channel and FRET channel. *Lower right*, DIC image showing the intestine lumen and cytoplasm area. *Red dash circles* represent the intestine lumen region. See also Fig. S5.

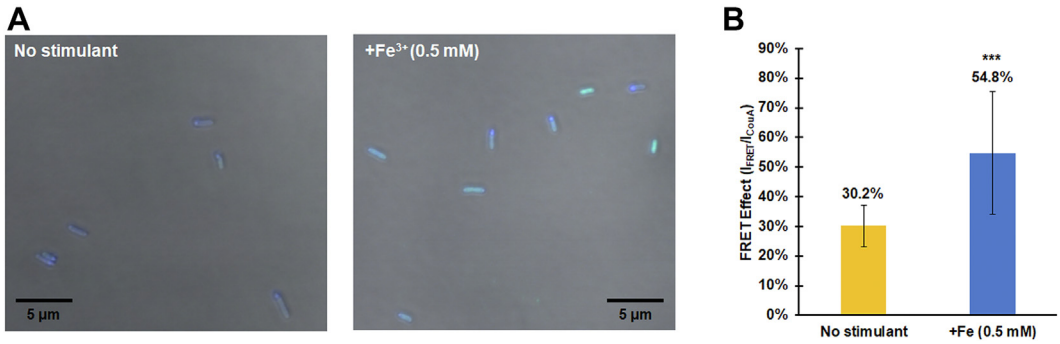

Figure 8. Single-cell FRET analysis monitors BasR activity in live *Escherichia coli* cells. *A*, merged images of *E. coli* MG1655 cells expressing BasR–G137CouA without stress stimulant (*left*) or treated with 0.5 mM Fe^{3+} (*right*). The merged images were acquired from CouA (*blue*), FRET (*green*), and DIC channels. *B*, FRET effect of the CouA–SYTO 9 pair calculated from 20 cells in the treated (0.5 mM Fe^{3+}) or untreated samples. Data shown are the mean of 20 datasets (collected from 20 cells) and presented as mean ± SD. *$p < 0.05$; **$p < 0.01$; and ***$p < 0.001$ (based on Student's *t* test). DIC, differential interference contrast.

Discussion

In recent decades, genetic codon expansion technique, which enables site-specific incorporation of genetically encoded unnatural amino acids (UAAs) into proteins, has revolutionized our ability to investigate the functions of proteins and their dynamics in living systems (73–76). However, the technique has not been leveraged to study transcription regulation during the stress adaptation in bacteria, which is essential to bacterial survival and infection. In this study, we encoded a bright FUAA CouA site specifically into the DBD of bacterial transcription regulator proteins and monitored the TF–promoter interaction in response to various stimulants and stresses based on the intermolecular FRET between the FUAA and the live cell DNA stain SYTO 9. As FRET represents almost the most accessible, sensitive, and super-resolved measurement for macromolecule associations, the assay system provides a powerful tool to monitor the adaptive gene regulation in living bacteria. We showed that the intermolecular FRET-based assay is capable of monitoring the binding of TF with its target promoters and activation of the corresponding regulatory systems in diverse signal transduction processes with specificity and sensitivity. Furthermore, the assay system is applicable to screen modulators of the regulatory systems of interests, report the activities of TFs in bacteria colonized in the *C. elegans* host, and is applicable in single-cell analysis. Hence, it provides a robust TF–promoter binding assay for investigating the complex and dynamic signal transduction processes in living cells, which are inaccessible by other methods currently available.

A common concern about intermolecular FRET-based biosensors is the occurrence of background noise and false positives caused by overproduction of the donor and acceptor fusions and cross-excitation of the acceptor by the excitation light of the donor. The problem of cross-excitation can be effectively solved by selecting a donor fluorophore with a large Stokes shift (77). The FRET donor we employed in this study, CouA, is a fluorophore with characteristic features ideal for FRET owing to its small size, high quantum field, and large Stokes shift (26). Indeed, no cross-excitation occurred in both the *in vitro* and *in vivo* FRET measurements established herein as demonstrated by a lack of fluorescence signal at 500 nm in the mixture of the CueR–F58CouA protein with a series concentration of SYTO 9 (Fig. S3*A*) and a modest increase of fluorescence intensity at 500 nm in the whole-cell suspension of BL21 mixed with varying amounts of SYTO 9 (Fig. S3*B*). A moderate condition for protein expression and CouA incorporation was applied for the whole-cell FRET-based assay. The level of CouA-incorporated TF proteins in the cell was determined to be in the range of 100 μg/ml, which affords sufficient fluorescence for FRET measurements but retains ample sensitivity as demonstrated by the assay of three different regulatory systems, CueR, BasSR, PhoPQ, in response to a broad range of signals and stresses tested. SYTO 9 is a common nucleic acid stain widely applied to identify and enumerate live bacteria in a population. Conceivably, the DNA content of a cell influences and determines the amount of SYTO 9 required to sufficiently cover the targeting promoters of the TF protein of interest. However, studies from McGoverin *et al.* (38) showed that nucleobase length and GC content of a bacterium did not significantly affect the SYTO 9 concentration required for enumeration of bacteria. It was proposed that the saturation concentration of SYTO 9 for a specific bacterial species was largely determined by the permeability of SYTO 9 to the bacterial cells and that micromolar (1 μM) SYTO 9 affords a robust signal for enumeration of common bacterial species including *E. coli* (38). In agreement with this notion, a limited extent of fluorescence intensity change was observed in the *E. coli* BL21 whole-cell suspension when 0.5 to 20 μM SYTO 9 was supplied. The SYTO 9 concentration we selected (7.5 μM) afforded sufficiently bright fluorescence for both fluorimeter and fluorescent microscopy analysis and retained ample sensitivity to report the FRET occurrence and its degree in response to stress signals. Hence, the intermolecular FRET-based assay we developed provides an accessible, robust, and generalizable approach to monitor TF–promoter interactions in living bacteria.

In most applications involving the site-specific incorporation of UAA for functional characterization of proteins, the 3D structure of the proteins is often known and required. Using

the CueR TF as an example, we demonstrated that structure-guided determination of CouA incorporation sites facilitated the establishment of the intermolecular FRET-based TF–promoter binding assay. However, crystal structures of many important transcription regulators and those of newly annotated regulators are unknown. Using BasR and PhoP as examples, we showed that simulated structures are reliable and applicable for determining the CouA incorporation sites for the assay. In these applications, 3D structures of BasR and PhoP were simulated by I-TASSER using the crystal structure of the corresponding homolog proteins, that is, *K. pneumoniae* PmrA and *M. tuberculosis* PhoP, respectively, as the template. Our further analysis showed that protein 3D structures predicted by the artificial intelligence–based programs such as AlphaFold and tFold (78, 79), in the absence of an existing template are also reliable and applicable for determination of the CouA incorporation sites (Fig. S7). Our studies demonstrated that the loop regions between α helices or β sheets in the DBD are optimal locations for CouA incorporation to monitor the TF–promoter interaction. However, certain amino acid residues, such as proline, are not tolerant to replacement by UAAs. Despite this, the fact that CouA can be incorporated into multiple locations in the loop regions of DBD to report the TF–promoter binding in CueR, BasR, and PhoP demonstrated the robustness and accessibility of the assay system we developed.

Two major classes of signal transduction systems exist in bacteria, the cytoplasmic one-component transcription regulators, which primarily sense intracellular signals, and the membrane-associated TCSs, which primarily sense membrane, periplasmic, and extracellular signals and stimulants. We showed that supplying inducing signals or stimulants in the assay suspension expressing the CouA-incorporated RR of TCSs elicited instant FRET. However, when the whole-cell assay was employed to monitor the binding of cytoplasmic TF CueR with its target promoters, supplementing the stimulant only in the assay suspension did not yield expected FRET signal even after 40 min incubation (data not shown). Instead, when the stimulants or modulators were supplied during CouA incorporation and protein expression, distinct FRET effect (in the presence of inducing signals) or abolishment of FRET (in the presence of signals inactivating the regulator) was observed. Hence, the stimulant application step needs to be adjusted depending on the types of the regulatory systems being investigated to enable proper signal perception.

In the past decades, the development of synthetic strategies has greatly accelerated the design and preparation of new FUAAs and nucleic acid dyes (80). With the development of these agents that display better fluorescence features, environmental sensitivity, and cell compatibility, the FRET-based assay for TF–promoter binding, and to a larger extent of protein–DNA interaction, will be continuously optimized for sensitive, robust, and broad applications. One potential application is to examine the kinetics of TF activity *in situ* during stress adaption process in living bacteria, which is currently limited by the speed of fluorescence scanning in the spectroscopy-based quantification method. However, it could be achieved through the single-cell analysis as we demonstrated employing time-lapse fluorescence microscope equipped with a microfluidic device.

Experimental procedures

Construction of plasmid for TF protein expression

DNA fragment encoding the TF protein of interest was obtained by PCR amplification using genomic DNA of *E. coli* MG1655 as the template. Primers used are listed in Table S2. The fragment and pET28a plasmid were both digested with NcoI and XhoI for 3 h at 37 °C. Following purification using the MiniBEST agarose gel DNA extraction kit (TaKaRa), the digested DNA fragment and pET28a were ligated using the quick ligation kit (NEB). The resulting construct was selected on LB agar plates supplemented with kanamycin (20 μg/ml) and verified by DNA sequencing (BGI). All plasmids constructed are listed in Table S3.

Amber codon mutation of the selected CouA incorporation sites

Each of the selected amino acid sites for CouA incorporation was mutated to a TAG amber codon by site-directed mutagenesis PCR. PCR was conducted using a pair of primers for the desired mutagenesis (Table S2) and pET28a-*cueR*, pET28a-*basR*, or pET28a-*phoP* plasmid as the template. PCR product was purified using MiniBEST agarose gel DNA extraction kit. Following DpnI digestion of the template at room temperature overnight, the PCR product was transformed into *E. coli* DH5α. The transformants were recovered on LB agar plates supplemented with kanamycin (20 μg/ml) at 37 °C overnight. Colonies recovered were verified by DNA sequencing (BGI).

CRISPR/Cas9-mediated deletion of P_{copA} and P_{cueO} in E. coli chromosome

Deletion of promoter regions of the *copA* and *cueO* genes in *E. coli* chromosome was achieved employing a CRISPR/Cas9-mediated approach developed by Zhao *et al.* (81) with modifications. *E. coli* BL21 (DE3) was electrotransformated with the pCAGO plasmid, which contains both SpCas9 and λ-RED to obtain BL21-pCAGO. A single colony of the resulting transformant was inoculated into LB medium supplemented with ampicillin (100 mg/ml) and grew overnight at 30 °C. About 100 μl of the overnight culture was inoculated into 10 ml fresh culture medium, and cells were grown at 30 °C with IPTG (0.1 mM) induction to an absorbance of 0.6 at 600 nm. The cells were collected and washed with cold double-distilled water for three times, generating competent cells for electroporation. An aliquot comprising 100 μl competent cells was mixed with 800 ng of the editing cassette, which encompasses 40 bp of upstream-homologous arm of *cueO* promoter region (-74 to -1) followed by the chloramphenicol-resistant gene, the N20PAM sequence (GTCCATCGAACCGAAGTAAGG), the other same upstream-homologous arm of *cueO* promoter region, and 40 bp downstream-homologous arm, in a 2 mm Gene Pulser cuvette (Bio-Rad), and was subjected to

electroporation at 2.3 kV. Following recovering the transformants by cultivation in LB medium for 2 h at 30 °C, the mixture was spread onto LB agar plate supplemented with ampicillin (100 mg/ml), chloramphenicol (25 mg/ml), and 1% glucose (to avoid the background expression of the Cas9 protein). Single colonies were collected and verified by colony PCR to obtain an authentic clone in which the *cueO* promoter region is replaced by the editing cassette. The confirmed colony was inoculated into LB medium supplemented with ampicillin (100 mg/ml), IPTG (0.1 mM), and L-arabinose (0.2%) at 30 °C overnight to enable expression of SpCas9 and the λ-RED recombinase. The cells were then spread on LB agar plates supplemented with ampicillin (100 mg/ml). Following colony PCR, desired colonies containing deletion of P*cueO* (AY7037) were verified by DNA sequencing (BGI). Deletion of the promoter region (-80 to -1) of *copA* gene in AY7038 was conducted following the same procedures except for the editing cassette sequence, which encompasses 40 bp of upstream-homologous arm of *copA* promoter region followed by the chloramphenicol-resistant gene, the N20PAM sequence, the other same 40 bp upstream-homologous arm of *copA* promoter region, and 40 bp downstream-homologous arm. After obtaining all desired genome modifications, the editing plasmid was cured by growing the resulting cells at 42 °C for 48 h.

CouA incorporation in TF proteins and purification of the resulting protein

The pET28a-*cueR*-F58TAG plasmid expressing a C-terminal His_6-tagged CueR–F58TAG was cotransformed with pEVOL-CouRS that contains $tRNA_{CUA}$ and aminoacyl $tRNA_{CUA}$ synthetase (26) into *E. coli* BL21 (DE3). Transformants were grown on an LB agar plate supplemented with kanamycin (20 μg/ml) and chloramphenicol (25 μg/ml). A single colony of the resulting transformant was inoculated into LB medium supplemented with kanamycin (20 μg/ml) and chloramphenicol (25 μg/ml) and grew overnight at 37 °C. About 1 ml of the overnight culture was inoculated into 100 ml of fresh culture medium, and cells were grown at 37 °C to an absorbance of 1.0 at 600 nm. Following induction of protein expression with 0.04% arabinose and 0.5 mM IPTG in the presence of 1 mM CouA (Shanghai VastPro Technology) for 12 h at 30 °C, cells were harvested by centrifugation (4000*g*) for 15 min. Cell pellet was resuspended in 10 ml lysis buffer (20 mM Tris–HCl, pH 8.0, and 2 M NaCl) and was subjected to sonication on ice. Cell debris was removed by centrifugation at 13,000*g* at 4 °C. About 1 ml Ni–nitrilotriacetic acid agarose (QIAGEN) was added to the collected supernatant, and the mixture was gently shaken at 4 °C for 2 h. Supernatant was removed by gravity column, and agarose beads were washed with 50 ml washing buffer (20 mM Tris–HCl, pH 8.0, 2 M NaCl, and 30 mM imidazole). CueR–F58CouA protein was eluted using elution buffer (20 mM Tris–HCl, pH 8.0, 2 M NaCl, and 500 mM imidazole). Purified protein was subsequently suspended in the buffer for binding assay (20 mM Tris–HCl, pH 8.0, and 150 mM NaCl) by buffer exchange through ultrafiltration at 4000*g*.

Verification of CouA incorporation by SDS-PAGE and LC–MS/MS

Purified CueR–F58CouA, BasR–D182CouA, and PhoP–A182CouA proteins were analyzed by SDS-PAGE electrophoresis. About 15 μl of each sample was loaded onto SDS-PAGE (Mini-PROTEAN Tetra system; Bio-Rad). Following electrophoresis for 60 min at room temperature, the gel was imaged under UV transilluminator (UVP) to record fluorescent band and then stained with Coomassie blue. The image of stained gel was recorded by Gel Doc XR+ imaging system (Bio-Rad). Gel slices corresponding to CueR–F58CouA (16.2 kDa), BasR–D182CouA (26.1 kDa), and PhoP–A182CouA (26.6 kDa) were excised and sent for eletrospray ionization LC–MS/MS (Dionex UltiMate 3000 RSLC nano Liquid Chromatography & Orbitrap Fusion Lumos Tribrid Mass Spectrometer).

TF protein structure prediction (PhoP as an example)

The 3D structure of TF or RR protein of TCSs was predicted *via* I-TASSER server. Amino acid sequences of these proteins were submitted to the server to yield a prediction on the secondary structure, solvent accessibility, and normalized *B*-factor. Ten templates that display the highest significance in the threading alignments from the PDB library were then identified. The server calculated two feasible models, model 1 and model 2 based on the 10 templates. The resulting prediction with a higher confidence score (C-score), that is, model 1 (0.95) in the case of the PhoP protein, was adopted to illustrate the structure of the protein in a PDB file.

Phosphorylation assay using Phos-tag SDS-PAGE

In vivo phosphorylation of BasR was examined using Phos-tag SDS-PAGE following our previous description (82) with minor modifications. *E. coli* MG1655 cell harboring pET28a-pBAD-*basR*-FLAG (AY7068) was inoculated into Mops minimum medium supplemented with kanamycin (20 μg/ml) and grew overnight at 37 °C. About 50 μl of the overnight culture was inoculated into 5 ml fresh Mops medium and grew at 37 °C for 4 h. Expression of BasR was induced with 1 mM arabinose for 1 h. The cells were collected by centrifugation at 4000*g*. The cells were washed with Mops medium supplemented with 0.1, 0.5, or 1 mM $FeCl_3$ twice and then cultivated in the corresponding medium for 1 h. About 1 ml of cells with an absorbance of ∼0.5 at 600 nm was collected for the subsequent analysis. The cell was washed with cold PBS twice and resuspended in 200 μl sample buffer (13 mM Tris, 0.2% SDS, 5% glycerol, 0.004% bromophenol blue, and pH 6.8) before being subjected to cell lysis by sonication. Following centrifugation at 13,000 rpm for 10 min at 4 °C, 25 μl of the sample was loaded onto the 10% Tris–Gly polyacrylamide gel containing 25 mM Phos-tag acrylamide (Wako) and 50 mM $MnCl_2$. The samples were separated by electrophoresis for 2 h at 4 °C. The gel was then washed with 50 ml transfer buffer containing 10 mM EDTA for 20 min to remove residual Mn^{2+}. Proteins on the gel were transferred onto a polyvinylidene difluoride membrane. The membrane was blocked with 5%

nonfat milk in Tris-buffered saline with Tween-20 buffer and incubated subsequently with monoclonal ANTI-FLAG M2 antibody (Sigma) and goat antimouse immunoglobulin G (H + L)-horseradish peroxidase conjugate (Bio-Rad). To detect FLAG-tagged protein bands, the membrane was submerged in the ECL Plus Western Blotting Detection Reagents (GE Healthcare) for 2 min and then subjected to the imaging system (UVITEC Cambridge) to record signals.

FRET-based CueR–promoter DNA binding assay in vitro

The 185 bp promoter region of *copA* gene (P_{copA}, −178 to +7 bp) was obtained by PCR using genomic DNA of *E. coli* MG1655 as the template. An additional DNA fragment (139 bp) located in the coding region of the *cueR* gene was also obtained by PCR and served as the negative control for the *in vitro* binding assay. About 10 μM purified CueR–F58CouA was mixed with 0.3 μM DNA fragment (P_{copA} or frag 1) in 100 μl assay buffer (20 mM Tris–HCl, 150 mM NaCl, pH 8.0) and incubated at room temperature for 15 min. About 15 μl SYTO 9 (50 μM in double-distilled water) was then added (final concentration of 7.5 μM). Following incubation for 15 min in dark, fluorescence spectrum of the mixture was recorded using Thermo Scientific Varioskan Flash spectral scanning multimode reader.

Whole-cell FRET measurement to detect in vivo $CueR_{CouA}$–$promoter_{SYTO\ 9}$ *binding*

A fresh single colony of *E. coli* cell (AY3660) harboring pET28a-*cueR*-F58TAG and pEVOL-CouRS was inoculated into LB medium supplemented with kanamycin (20 μg/ml) and chloramphenicol (25 μg/ml) and grew overnight at 37 °C. About 75 μl of the overnight culture was inoculated to 7.5 ml fresh medium to subculture the bacteria. Following culturing at 37 °C for 4 h, CouA incorporation and expression of CueR–F58CouA (or CueR–T27CouA, CueR–Y39CouA, CueR–Q74CouA) was induced mildly by supplementing 0.5 mM IPTG, 0.4% arabinose, and 1 mM CouA at 37 °C for 4 h. Metal ion (stimulating signals) of 0.1 mM $CuSO_4$, 0.02 mM $MnCl_2$, or 0.02 mM $NiCl_2$ (final concentration) was also added. Approximately 8×10^9 cells were harvested and washed twice with PBS buffer. Following centrifugation at 4000*g* for 15 min at 4 °C, cell pellet was resuspended in 600 μl of PBS. About 85 μl of the suspension was added in each of six wells (three wells for control group and three wells for experimental group) on a 96-well black plate preloaded with 15 μl of 50 μM SYTO 9 and incubated for 15 min at room temperature in the dark before being subjected to fluorescence recording.

In vivo $BasR_{CouA}$–$promoter_{SYTO\ 9}$ *binding assay*

Plasmid pET28a-pBAD-*basR*-D182TAG, G137TAG, E146TAG, or S167TAG was cotransformed with pEVOL-CouRS into *E. coli* MG1655 *ΔbasR* strain, resulting in AY7064, AY7065, AY7066, and AY7067 constructs, respectively. Culture conditions for mild protein induction and CouA incorporation were similar to that described for the $CueR_{CouA}$–$promoter_{SYTO\ 9}$ binding assay except that (1) the inoculum was cultured in Mops minimum medium at 37 °C for 4 h before induction and (2) the induction was conducted in the presence of 0.9% arabinose and 1 mM CouA at 37 °C for 5 h. Approximately 3.5×10^{10} cells were harvested and washed twice with fresh Mops medium. The cells were resuspended in Mops medium supplemented with 0.5 mM $FeCl_3$ as the inducing signal for the BasSR TCS and shaken for 1 h at 37 °C. After centrifugation at 4000*g* for 15 min at 4 °C, cell pellet was resuspended in 600 μl of PBS. The sample preparation and fluorescence spectrum recording were performed as described in the $CueR_{CouA}$–$promoter_{SYTO\ 9}$ binding assay.

In vivo $PhoP_{CouA}$–$promoter_{SYTO\ 9}$ *binding assay*

The pET28a-*phoP*-S137TAG, D145TAG, or A182TAG plasmid was cotransformed with pEVOL-CouRS into *E. coli* BL21 (DE3), resulting in AY3707, AY3708, and AY3709 constructs, respectively. Culture conditions for mild protein induction and CouA incorporation were similar to that described for the $CueR_{CouA}$–promoter $DNA_{SYTO\ 9}$ binding assay except that (1) the induction was conducted in the presence of 0.5 mM IPTG, 0.4% arabinose, and 1 mM CouA at 37 °C for 5 h and (2) the stimulants for the PhoPQ system were applied prior to fluorescence signal recording rather than during the induction. Approximately 6×10^9 cells were harvested and subjected to sample preparation. Following incubation of 85 μl of cell suspension containing mildly induced PhoP–CouA protein and 15 μl of SYTO 9 (50 μM) at room temperature for 15 min in the dark, different stimuli were added in the buffer. About 1 mM of $MgCl_2$ was added to the cell suspension before adding other stimulants. EDTA, polymyxin B, tryptophan, indole, IAA, and gentamycin were added at the designated concentrations in the text. The suspension is subjected to fluorescence spectrum recording as described previously. Zero time is defined as the fluorescence of the assay system recorded immediately following the addition of stimulants.

Fluorescence spectroscopy and FRET effect quantification

Fluorescence spectra of the assay suspension described previously were recorded using Thermo Scientific Varioskan Flash spectral scanning multimode reader at 25 °C. The excitation wavelength was fixed at 360 nm, and the scanning wavelength was recorded from 400 to 550 nm. Degree of the FRET effect was quantified by the ratio of

$$F_E = I_A / I_D \quad (1)$$

where I_A is the emission fluorescence intensity of the acceptor SYTO 9 at 500 nm, and I_D is the emission fluorescence intensity of CouA at 450 nm following several previous descriptions (83–86).

The Förster radius R_0 is the Förster distance, which is the distance between the FRET donor and acceptor when the

energy transfer efficiency is 50%. R_0 is calculated from the equation (87):

$$R_0^6 = \left(\frac{9000\ (\ln 10) \cdot \kappa^2 \cdot Q_D \cdot J(\lambda)}{128 \cdot \pi^5 \cdot N_A \cdot n^4}\right) (\text{in } \text{Å}^6) \quad (2)$$

where k^2 is the orientation factor in resonance energy transfer, Q_D is the quantum yield of the donor in the absence of acceptor, N_A is Avogadro's number, n is the refractive index of the medium, and $J(\lambda)$ is the overlap integral. To calculate this equation, k_2 is designated as 2/3, Q_D as 0.63, n as 1.4, and N_A as $6.02214076 \times 10^{23}$. The $J(\lambda)$ is calculated by (87):

$$J(\lambda) = \frac{\int_0^\infty F_D(\lambda)\varepsilon_A(\lambda)\lambda^4 d\lambda}{\int_0^\infty F_D(\lambda) d\lambda} \quad (3)$$

where F_D is the emission spectrum of the donor, $\varepsilon_A(\lambda)$ is the molar extinction coefficient of the acceptor at λ, which is 50,000 cm^{-1} M^{-1} for SYTO 9.

Preparation of E. coli *cells expressing PhoP–A182CouA and its uptake by the* C. elegans *DA597*

C. elegans phm-2(-) mutant strain DA597, which lost the grinder function, was obtained from the Caenorhabditis Genetics Center. *E. coli* BL21 cells expressing PhoP–A182CouA (AY3706) was cultured in LB medium supplemented with kanamycin (20 μg/ml) and chloramphenicol (25 μg/ml) at 37 °C for 5 h in the presence of 0.5 mM IPTG, 0.4% arabinose, and 1 mM CouA. Cells were collected and washed with M9 buffer (0.3% KH_2PO_4, 0.6% Na_2HPO_4, 0.5% NaCl, and 1 mM $MgSO_4$). About 5 μl of 50 μM SYTO 9 was added in 1 ml cell suspension (final concentration of 0.25 μM), which was then incubated for 15 min in the dark to enable the entry of SYTO 9 into *E. coli* cells. The suspension was washed with 1 ml M9 buffer for three times and finally resuspended in 100 μl of M9 buffer and was then placed in the center of a 60 mm NGM agar plate (0.25% peptone, 0.3% NaCl, 1.7% Bacto-agar, 1 mM $CaCl_2$, 1 mM $MgSO_4$, 5 mg cholesterol, and 25 mM phosphate buffer) in a circle (20 mm diameter) as food for the *C. elegans* DA597 strain. This plate is termed as AY3706-NGM plate. The eggs of DA597 were then seeded onto NGM agar plate containing *E. coli* OP50 (OP50-NGM) and fed for 48 h at 20 °C. Ten L4 stage larva grown on the OP50-NGM plate were then transferred to the AY3706-NGM plate and fed with the AY3706 bacteria for 2 h at 20 °C before being subjected to fluorescent microscopy imaging.

FRET recording using confocal fluorescent microscope

The larva grown on the AY3706-NGM plate described previously following 2-h incubation were placed onto an agarose pad containing 3% agarose and 4% 2,3-butanedione monoxime on a microscope slide. Fluorescence signal emitted from the larva was recorded using Zeiss LSM 710 confocal microscope using 40× oil immersion objective lens. The sample was excited at 405 nm, and the emission fluorescence of CouA was recorded from 420 to 480 nm. To record the emission fluorescence of SYTO 9, the sample was excited at 488 nm and emission fluorescence was recorded from 490 to 600 nm. To record the fluorescence effected by FRET, the sample was excited at 405 nm by laser, and emission fluorescence was recorded from 490 to 600 nm.

Data availability

The mass spectrometry proteomics data have been deposited to the ProteomeXchange Consortium *via* the PRIDE (88) partner repository with the dataset identifier PXD030973 (username: reviewer_pxd030973@ebi.ac.uk; password: OV7ZS40g).

Supporting information—This article contains supporting information.

Acknowledgments—The *C. elegans* strains used in this study were provided by the Caenorhabditis Genetics Center, which is funded by the National Institutes of Health Office of Research Infrastructure Programs (grant no.: P40 OD010440Z). We thank Dr Chenghao Bi (Tianjin Institute of Industrial Biotechnology, Chinese Academy of Sciences) for the gift of the pCAGO plasmid. We thank Proteomics and Metabolomics Core, Centre for PanorOmic Sciences, in the University of Hong Kong for their help and support on proteomics analysis.

Author contributions—P. W., Z. X., and A. Y. conceptualization; P. W., Z. X., X. L., C. W., J. W., and A. Y. methodology; P. W. and Z. C. formal analysis; P. W. and G. Z. investigation; X. L., C. W., C. Z., J. W., and A. Y. resources; P. W. writing–original draft; C. Z., H. Z., and A. Y. writing–review & editing; H. Z. and A. Y. supervision; A. Y. project administration; H. Z. and A. Y. funding acquisition.

Funding and additional information—This study was supported by grants from Hong Kong Government Food and Health Bureau Health and Medical Research Fund (grant no.: 18171042; to A. Y.); Hong Kong University Grants Council General Research Fund (grant no.: 17127918; to A. Y.); HKU Seed Fund for Basic Research (grant no.: 201910159291; to A. Y.); and Ministry of Science and Technology (Synthetic Biology Special Project of National Key R&D Program; grant no.: 2019YFA0906000; to H. Z.). The content is solely the responsibility of the authors and does not necessarily represent the official views of the National Institutes of Health.

Conflict of interest—The authors declare that they have no conflicts of interest with the contents of this article.

Abbreviations—The abbreviations used are: CouA, L-(7-hydroxycoumarin-4-yl) ethylglycine; DBD, DNA-binding domain; FUAA, fluorescent unnatural amino acid; HK, histidine kinase; IAA, indole-3-acetic acid; PDB, Protein Data Bank; RR, response regulator; TCS, two-component system; TF, transcription factor; UAA, unnatural amino acid.

References

1. Fang, F. C., Frawley, E. R., Tapscott, T., and Vazquez-Torres, A. (2016) Bacterial stress responses during host infection. *Cell Host Microbe* **20**, 133–143

2. Ron, E. Z. J. T.p. (2006) Bacterial stress response. *The Prokaryotes*. https://doi.org/10.1007/0-387-30742-7_32
3. Cai, Y. H., and Huang, H. (2012) Advances in the study of protein-DNA interaction. *Amino Acids* **43**, 1141–1146
4. Dey, B., Thukral, S., Krishnan, S., Chakrobarty, M., Gupta, S., Manghani, C., *et al.* (2012) DNA-Protein interactions: methods for detection and analysis. *Mol. Cell Biochem.* **365**, 279–299
5. Vossen, K. M., and Fried, M. G. J. A.b. (1997) Sequestration StabilizeslacRepressor–DNA complexes during gel electrophoresis. *Anal. Biochem.* **245**, 85–92
6. Fried, M. G., and Liu, G. (1994) Molecular sequestration stabilizes CAP-DNA complexes during polyacrylamide gel electrophoresis. *Nucl. Acids Res.* **22**, 5054–5059
7. Oehler, S., Alex, R., and Barker, A. J. A.b. (1999) Is nitrocellulose filter binding really a universal assay for protein–DNA interactions? *Anal. Biochem.* **268**, 330–336
8. Hampshire, A. J., Rusling, D. A., Broughton-Head, V. J., and Fox, K. R. (2007) Footprinting: a method for determining the sequence selectivity, affinity and kinetics of DNA-binding ligands. *Methods* **42**, 128–140
9. Oda, M., and Nakamura, H. (2000) Thermodynamic and kinetic analyses for understanding sequence-specific DNA recognition. *Genes Cells* **5**, 319–326
10. Pillet, F., Sanchez, A., Formosa, C., Severac, M., Trevisiol, E., Bouet, J. Y., *et al.* (2013) Dendrimer functionalization of gold surface improves the measurement of protein-DNA interactions by surface plasmon resonance imaging. *Biosens. Bioelectron.* **43**, 148–154
11. Ellington, A. D., and Szostak, J. W. (1990) *In vitro* selection of RNA molecules that bind specific ligands. *Nature* **346**, 818–822
12. Myers, K. S., Park, D. M., Beauchene, N. A., and Kiley, P. J. (2015) Defining bacterial regulons using ChIP-seq. *Methods* **86**, 80–88
13. Förster, T. J. A.d.p. (1948) Zwischenmolekulare energiewanderung und fluoreszenz. *Annalen der physik* **437**, 55–75
14. Jares-Erijman, E. A., and Jovin, T. M. (2003) FRET imaging. *Nat. Biotechnol.* **21**, 1387–1395
15. Roy, R., Hohng, S., and Ha, T. (2008) A practical guide to single-molecule FRET. *Nat. Met.* **5**, 507–516
16. Stryer, L. (1978) Fluorescence energy-transfer as a spectroscopic ruler. *Annu. Rev. Biochem.* **47**, 819–846
17. Periasamy, A., and Day, R. (2011) *Molecular Imaging: FRET Microscopy and Spectroscopy*, Oxford University Press, Inc, New York, NY
18. Jares-Erijman, E. A., and Jovin, T. M. (2006) Imaging molecular interactions in living cells by FRET microscopy. *Curr. Opin. Chem. Biol.* **10**, 409–416
19. Sekar, R. B., and Periasamy, A. (2003) Fluorescence resonance energy transfer (FRET) microscopy imaging of live cell protein localizations. *J. Cell Biol* **160**, 629–633
20. Park, H., Kang, H., Ko, W., Lee, W., Jo, K., and Lee, H. S. (2015) FRET-based analysis of protein-nucleic acid interactions by genetically incorporating a fluorescent amino acid. *Amino Acids* **47**, 729–734
21. Schärfen, L., and Schlierf, M. J. M. (2019) Real-time monitoring of protein-induced DNA conformational changes using single-molecule FRET. *Methods* **169**, 11–20
22. Zhang, S., Metelev, V., Tabatadze, D., Zamecnik, P. C., and Bogdanov, A. (2008) Fluorescence resonance energy transfer in near-infrared fluorescent oligonucleotide probes for detecting protein–DNA interactions. *Proc. Natl. Acad. Sci. U. S. A.* **105**, 4156–4161
23. Cremazy, F. G. E., Manders, E. M. M., Bastiaens, P. I. H., Kramer, G., Hager, G. L., van Munster, E. B., *et al.* (2005) Imaging *in situ* protein-DNA interactions in the cell nucleus using FRET-FLIM. *Exp. Cell Res.* **309**, 390–396
24. Wiederschain, G. Y. (2011). In *The Molecular Probes Handbook. A Guide to Fluorescent Probes and Labeling Technologies*, Springer, Dordrecht, Netherlands
25. Wang, L., Brock, A., Herberich, B., and Schultz, P. G. (2001) Expanding the genetic code of *Escherichia coli*. *Science* **292**, 498–500
26. Wang, J., Xie, J., and Schultz, P. G. (2006) A genetically encoded fluorescent amino acid. *J. Am. Chem. Soc.* **128**, 8738–8739
27. Summerer, D., Chen, S., Wu, N., Deiters, A., Chin, J. W., and Schultz, P. G. (2006) A genetically encoded fluorescent amino acid. *Proc. Natl. Acad. Sci. U. S. A.* **103**, 9785–9789
28. Speight, L. C., Muthusamy, A. K., Goldberg, J. M., Warner, J. B., Wissner, R. F., Willi, T. S., *et al.* (2013) Efficient synthesis and *in vivo* incorporation of acridon-2-ylalanine, a fluorescent amino acid for lifetime and Forster resonance energy transfer/luminescence resonance energy transfer studies. *J. Am. Chem. Soc.* **135**, 18806–18814
29. Lampkowski, J. S., Uthappa, D. M., and Young, D. D. (2015) Site-specific incorporation of a fluorescent terphenyl unnatural amino acid. *Bioorg. Med. Chem. Lett.* **25**, 5277–5280
30. Luo, J., Uprety, R., Naro, Y., Chou, C., Nguyen, D. P., Chin, J. W., *et al.* (2014) Genetically encoded optochemical probes for simultaneous fluorescence reporting and light activation of protein function with two-photon excitation. *J. Am. Chem. Soc.* **136**, 15551–15558
31. Lee, H. S., Guo, J. T., Lemke, E. A., Dimla, R. D., and Schultz, P. G. (2009) Genetic incorporation of a small, environmentally sensitive, fluorescent probe into proteins in *Saccharomyces cerevisiae*. *J. Am. Chem. Soc.* **131**, 12921–12923
32. Stoyanov, J. V., Hobman, J. L., and Brown, N. L. (2001) CueR (YbbI) of *Escherichia coli* is a MerR family regulator controlling expression of the copper exporter CopA. *Mol. Microbiol.* **39**, 502–511
33. Outten, F. W., Outten, C. E., Hale, J., and O'Halloran, T. V. (2000) Transcriptional activation of an *Escherichia coli* copper Efflux regulon by the chromosomal MerR homologue, CueR. *J. Biol. Chem.* **275**, 31024–31029
34. Yamamoto, K., and Ishihama, A. (2005) Transcriptional response of *Escherichia coli* to external copper. *Mol. Microbiol.* **56**, 215–227
35. Philips, S. J., Canalizo-Hernandez, M., Yildirim, I., Schatz, G. C., Mondragon, A., and O'Halloran, T. V. (2015) Allosteric transcriptional regulation *via* changes in the overall topology of the core promoter. *Science* **349**, 877–881
36. Fang, C., Philips, S. J., Wu, X., Chen, K., Shi, J., Shen, L., *et al.* (2021) CueR activates transcription through a DNA distortion mechanism. *Nat. Chem. Biol.* **17**, 57–64
37. Elowitz, M. B., Surette, M. G., Wolf, P.-E., Stock, J. B., and Leibler, S. (1999) Protein mobility in the cytoplasm of *Escherichia coli*. *J. Biol. Chem.* **181**, 197–203
38. McGoverin, C., Robertson, J., Jonmohamadi, Y., Swift, S., and Vanholsbeeck, F. (2020) Species dependence of SYTO 9 staining of bacteria. *Front. Microbiol.* **11**, 2149
39. Xu, Z., Wang, P., Wang, H., Yu, Z. H., Au-Yeung, H. Y., Hirayama, T., *et al.* (2019) Zinc excess increases cellular demand for iron and decreases tolerance to copper in *Escherichia coli*. *J. Biol. Chem.* **294**, 16978–16991
40. Wösten, M. M., Kox, L. F., Chamnongpol, S., Soncini, F. C., and Groisman, E. A. J. C. (2000) A signal transduction system that responds to extracellular iron. *Cell* **103**, 113–125
41. Kato, A., Chen, H. D., Latifi, T., and Groisman, E. A. (2012) Reciprocal control between a bacterium's regulatory system and the modification status of its lipopolysaccharide. *Mol. Cell* **47**, 897–908
42. Ogasawara, H., Shinohara, S., Yamamoto, K., and Ishihama, A. (2012) Novel regulation targets of the metal-response BasS-BasR two-component system of Escherichia coli. *Microbiology (Reading)* **158**, 1482–1492
43. Roy, A., Kucukural, A., and Zhang, Y. (2010) I-TASSER: a unified platform for automated protein structure and function prediction. *Nat. Protoc.* **5**, 725–738
44. Yang, J., Yan, R., Roy, A., Xu, D., Poisson, J., and Zhang, Y. (2015) The I-TASSER suite: protein structure and function prediction. *Nat. Met.* **12**, 7–8
45. Yang, J., and Zhang, Y. (2015) I-TASSER server: new development for protein structure and function predictions. *Nucl. Acids Res.* **43**, W174–181
46. Blattner, F. R., Plunkett, G., 3rd, Bloch, C. A., Perna, N. T., Burland, V., Riley, M., *et al.* (1997) The complete genome sequence of *Escherichia coli* K-12. *Science* **277**, 1453–1462
47. Hoch, J. A. (2000) Two-component and phosphorelay signal transduction. *Curr. Opin. Microbiol.* **3**, 165–170
48. Stock, A. M., Robinson, V. L., and Goudreau, P. N. (2000) Two-component signal transduction. *Annu. Rev. Biochem.* **69**, 183–215

49. Prost, L. R., Daley, M. E., Le Sage, V., Bader, M. W., Le Moual, H., Klevit, R. E., *et al.* (2007) Activation of the bacterial sensor kinase PhoQ by acidic pH. *Mol. Cell* **26**, 165–174
50. Bader, M. W., Sanowar, S., Daley, M. E., Schneider, A. R., Cho, U., Xu, W., *et al.* (2005) Recognition of antimicrobial peptides by a bacterial sensor kinase. *Cell* **122**, 461–472
51. Vescovi, E. G., Ayala, Y. M., Di Cera, E., and Groisman, E. A. (1997) Characterization of the bacterial sensor protein PhoQ. Evidence for distinct binding sites for Mg2+ and Ca2+. *J. Biol. Chem.* **272**, 1440–1443
52. Yuan, J., Jin, F., Glatter, T., and Sourjik, V. (2017) Osmosensing by the bacterial PhoQ/PhoP two-component system. *Proc. Natl. Acad. Sci. U. S. A.* **114**, E10792–E10798
53. Véscovi, E. G., Soncini, F. C., and Groisman, E. A. J. C. (1996) Mg2+ as an extracellular signal: environmental regulation of *Salmonella* virulence. *Cell* **84**, 165–174
54. Beier, D., and Gross, R. (2006) Regulation of bacterial virulence by two-component systems. *Curr. Opin. Microbiol.* **9**, 143–152
55. Capra, E. J., and Laub, M. T. (2012) Evolution of two-component signal transduction systems. *Annu. Rev. Microbiol.* **66**, 325–347
56. Francis, V. I., and Porter, S. L. (2019) Multikinase networks: Two-component signaling networks integrating multiple stimuli. *Annu. Rev. Microbiol.* **73**, 199–223
57. Martín-Mora, D., Fernández, M., Velando, F., Ortega, Á., Gavira, J. A., Matilla, M. A., *et al.* (2018) Functional annotation of bacterial signal transduction systems: Progress and challenges. *Int. J. Mol. Sci.* **19**, 3755
58. Matilla, M. A., Velando, F., Martín-Mora, D., Monteagudo-Cascales, E., and Krell, T. (2021) A catalogue of signal molecules that interact with sensor kinases, chemoreceptors and transcriptional regulators. *FEMS Microbiol. Rev.* **46**, fuab043
59. Bianco, C., Imperlini, E., Calogero, R., Senatore, B., Pucci, P., and Defez, R. (2006) Indole-3-acetic acid regulates the central metabolic pathways in *Escherichia coli*. *Microbiology (Reading)* **152**, 2421–2431
60. Dwyer, D. J., Belenky, P. A., Yang, J. H., MacDonald, I. C., Martell, J. D., Takahashi, N., *et al.* (2014) Antibiotics induce redox-related physiological alterations as part of their lethality. *Proc. Natl. Acad. Sci. U. S. A.* **111**, E2100–E2109
61. Khodursky, A. B., Peter, B. J., Cozzarelli, N. R., Botstein, D., Brown, P. O., and Yanofsky, C. (2000) DNA microarray analysis of gene expression in response to physiological and genetic changes that affect tryptophan metabolism in *Escherichia coli*. *Proc. Natl. Acad. Sci. U. S. A.* **97**, 12170–12175
62. Bansal, T., Englert, D., Lee, J., Hegde, M., Wood, T. K., and Jayaraman, A. (2007) Differential effects of epinephrine, norepinephrine, and indole on *Escherichia coli* O157:H7 chemotaxis, colonization, and gene expression. *Infect. Immun.* **75**, 4597–4607
63. Garsin, D. A., Sifri, C. D., Mylonakis, E., Qin, X., Singh, K. V., Murray, B. E., *et al.* (2001) A simple model host for identifying Gram-positive virulence factors. *Proc. Natl. Acad. Sci. U. S. A.* **98**, 10892–10897
64. Dirksen, P., Marsh, S. A., Braker, I., Heitland, N., Wagner, S., Nakad, R., *et al.* (2016) The native microbiome of the nematode Caenorhabditis elegans: gateway to a new host-microbiome model. *BMC Biol.* **14**, 1–16
65. Vasquez-Rifo, A., Ricci, E. P., and Ambros, V. (2020) Pseudomonas aeruginosa cleaves the decoding center of Caenorhabditis elegans ribosomes. *PLoS Biol.* **18**, e3000969
66. Tan, M. W., Mahajan-Miklos, S., and Ausubel, F. M. (1999) Killing of *Caenorhabditis elegans* by *Pseudomonas aeruginosa* used to model mammalian bacterial pathogenesis. *Proc. Natl. Acad. Sci. U. S. A.* **96**, 715–720
67. Kurz, C. L., and Ewbank, J. J. (2000) *Caenorhabditis elegans* for the study of host-pathogen interactions. *Trends Microbiol.* **8**, 142–144
68. Vadyvaloo, V., Viall, A. K., Jarrett, C. O., Hinz, A. K., Sturdevant, D. E., and Joseph Hinnebusch, B. (2015) Role of the PhoP-PhoQ gene regulatory system in adaptation of *Yersinia pestis* to environmental stress in the flea digestive tract. *Microbiology (Reading)* **161**, 1198–1210
69. Rychlik, I., and Barrow, P. A. (2005) *Salmonella* stress management and its relevance to behaviour during intestinal colonisation and infection. *FEMS Microbiol. Rev.* **29**, 1021–1040
70. Porcheron, G., Schouler, C., and Dozois, C. M. (2016) Survival games at the dinner table: regulation of enterobacterial virulence through nutrient sensing and acquisition. *Curr. Opin. Microbiol.* **30**, 98–106
71. Avery, L. (1993) The genetics of feeding in *Caenorhabditis elegans*. *Genetics* **133**, 897–917
72. Vaknin, A., and Berg, H. C. (2004) Single-cell FRET imaging of phosphatase activity in the Escherichia coli chemotaxis system. *Proc. Natl. Acad. Sci. U. S. A.* **101**, 17072–17077
73. Vargas-Rodriguez, O., Sevostyanova, A., Soll, D., and Crnkovic, A. (2018) Upgrading aminoacyl-tRNA synthetases for genetic code expansion. *Curr. Opin. Chem. Biol.* **46**, 115–122
74. Wang, Q., Parrish, A. R., and Wang, L. (2009) Expanding the genetic code for biological studies. *Chem. Biol.* **16**, 323–336
75. Lv, X., Yu, Y., Zhou, M., Hu, C., Gao, F., Li, J., *et al.* (2015) Ultrafast photoinduced electron transfer in green fluorescent protein bearing a genetically encoded electron acceptor. *J. Am. Chem. Soc.* **137**, 7270–7273
76. Zhang, W. H., Otting, G., and Jackson, C. J. (2013) Protein engineering with unnatural amino acids. *Curr. Opin. Struct. Biol.* **23**, 581–587
77. Santana-Calvo, C., Romero, F., López-González, I., and Nishigaki, T. (2018) Robust evaluation of intermolecular FRET using a large Stokes shift fluorophore as a donor. *BioTechniques* **65**, 211–218
78. Shen, T., Wu, J. X., Lan, H. D., Zheng, L. Z., Pei, J. G., Wang, S., *et al.* (2021) When homologous sequences meet structural decoys: accurate contact prediction by tFold in CASP14-(tFold for CASP14 contact prediction). *Proteins* **89**, 1901–1910
79. Jumper, J., Evans, R., Pritzel, A., Green, T., Figurnov, M., Ronneberger, O., *et al.* (2021) Highly accurate protein structure prediction with AlphaFold. *Nature* **596**, 583–589
80. Rombouts, K., Braeckmans, K., and Remaut, K. (2016) Fluorescent labeling of plasmid DNA and mRNA: gains and losses of current labeling strategies. *Bioconjug. Chem.* **27**, 280–297
81. Zhao, D. D., Feng, X., Zhu, X. N., Wu, T., Zhang, X. L., and Bi, C. H. (2017) CRISPR/Cas9-assisted gRNA-free one-step genome editing with no sequence limitations and improved targeting efficiency. *Sci. Rep.* **7**, 1–9
82. Fung, D. K., Ma, Y., Xia, T., Luk, J. C., and Yan, A. (2016) Signaling by the heavy-metal sensor CusS involves rearranged helical interactions in specific transmembrane regions. *Mol. Microbiol.* **100**, 774–787
83. Huang, S.-M., Yang, F., Cai, B.-Y., He, Q.-T., Liu, Q., Qu, C.-X., *et al.* (2019) Genetically encoded fluorescent amino acid for monitoring protein Interactions through FRET. *Anal. Chem.* **91**, 14936–14942
84. Glasscock, J. M., Zhu, Y. J., Chowdhury, P., Tang, J., and Gai, F. (2008) Using an amino acid fluorescence resonance energy transfer pair to probe protein unfolding: application to the villin headpiece subdomain and the LysM domain. *Biochemistry* **47**, 11070–11076
85. Ko, W., Kim, S., Lee, S., Jo, K., and Lee, H. S. (2016) Genetically encoded FRET sensors using a fluorescent unnatural amino acid as a FRET donor. *Rsc Adv.* **6**, 78661–78668
86. Kajihara, D., Abe, R., Iijima, I., Komiyama, C., Sisido, M., and Hohsaka, T. (2006) FRET analysis of protein conformational change through position-specific incorporation of fluorescent amino acids. *Nat. Met.* **3**, 923–929
87. Lakowicz, J. R. (2013) *Principles of Fluorescence Spectroscopy*, Springer Science+Business Media, LLC, New York, NY
88. Perez-Riverol, Y., Bai, J., Bandla, C., García-Seisdedos, D., Hewapathirana, S., Kamatchinathan, S., *et al.* (2022) The PRIDE database resources in 2022: a hub for mass spectrometry-based proteomics evidences. *Nucl. Acids Res.* **50**, D543–D552